

# Macrophage WDFY3 mitigates autoimmunity by enhancing efferocytosis and suppressing T cell activation in mice

Received: 8 August 2024

Accepted: 25 August 2025

Published online: 30 September 2025



Xun Wu<sup>1</sup>✉, Ziyi Wang<sup>1</sup>, Katherine R. Croce<sup>2</sup>, Fang Li<sup>1</sup>, Jian Cui<sup>1</sup>, Vivette D. D'Agati<sup>3,4</sup>, Rajesh K. Soni<sup>3</sup>, Ira Tabas<sup>3,5,6</sup>, Ai Yamamoto<sup>2,3</sup> & Hanrui Zhang<sup>1</sup>✉

Efficient efferocytosis is crucial for immune homeostasis. Conversely, excessive apoptotic cell (AC) death and impaired macrophage efferocytosis lead to autoantigen release, autoantibody production, and immune activation. It is unclear whether immunogenic autoantigens from impaired clearance are the sole cause of autoimmunity or if AC efferocytosis directly alters macrophage function, affecting T cell activation and amplifying autoimmunity. Our prior work identified WDFY3 as essential for macrophage efferocytosis. Here, we demonstrate that myeloid *Wdfy3* knockout exacerbates autoimmunity in young mice receiving systemic AC injections and middle-aged mice developing autoreactivity. Mechanistically, myeloid *Wdfy3* deletion impairs efferocytosis, increasing autoantigen availability, and augments MHC-II-mediated antigen presentation and cytokine dysregulation, thereby promoting CD4<sup>+</sup> T cell activation. In contrast, WDFY3 overexpression enhances efferocytosis, suppresses macrophage-mediated CD4<sup>+</sup> T cell activation, and mitigates autoimmunity. Thus, macrophage WDFY3 functions as a protective factor against autoimmunity. Enhancing macrophage efferocytosis and reprogramming macrophage responses to ACs may represent promising strategies to limit autoimmune disorders and age-associated autoimmunity.

Efficient efferocytosis of dying cells by phagocytes, mainly macrophages, is essential for maintaining homeostasis<sup>1,2</sup>. When the burden of apoptotic cells (AC) exceeds the clearance capacity of efferocytosis, uncleared ACs undergo secondary necrosis, releasing intracellular contents that become persistent immunogenic stimuli. Autoantigens from necrotic cells are processed and presented by antigen-presenting cells, including macrophages, via MHC-II, leading to aberrant CD4<sup>+</sup> T cell activation. Activated T cells in turn activate B cells to produce autoantibodies<sup>3,4</sup>. These autoantibodies can form immune complexes

that deposit in organs, including the kidneys, triggering inflammation and pathological damage<sup>5</sup>. Additionally, inflammatory cytokines released due to defective efferocytosis promote dendritic cell (DC) maturation and loss of tolerogenic function, stimulating pro-inflammatory T cell responses and perpetuating a cycle of autoimmunity<sup>6</sup>. Thus, impaired AC clearance serves as a critical driver of tolerance loss and immune activation underlying autoimmunity<sup>1,7</sup>.

Excessive AC death and impaired efferocytosis are observed in patients with systemic lupus erythematosus<sup>8–11</sup>. Impaired efferocytosis

<sup>1</sup>Cardiometabolic Genomics Program, Division of Cardiology, Department of Medicine, Columbia University Irving Medical Center, New York, NY 10032, USA.

<sup>2</sup>Department of Neurology, Columbia University, New York, NY 10032, USA. <sup>3</sup>Department of Pathology and Cell Biology, Columbia University, New York, NY 10032, USA. <sup>4</sup>Renal Pathology Laboratory, Columbia University Irving Medical Center, New York, NY 10032, USA. <sup>5</sup>Department of Medicine, Columbia University Irving Medical Center, New York, NY 10032, USA. <sup>6</sup>Department of Physiology and Cellular Biophysics, Columbia University Irving Medical Center, New York, NY 10032, USA. ✉e-mail: [xw2698@cumc.columbia.edu](mailto:xw2698@cumc.columbia.edu); [hz2418@cumc.columbia.edu](mailto:hz2418@cumc.columbia.edu)

is also evident in macrophages from aged mice compared to their younger counterparts, indicating an age-related decline in clearance efficiency<sup>12,13</sup>. Experimental studies establish that mice lacking genes involved in regulating efferocytosis have impaired clearance of ACs and develop lupus-like autoimmunity or spontaneous autoimmunity in aging<sup>14–18</sup>, including genes coding for efferocytic receptors such as MERTK or TIM4<sup>14,15</sup>, scavenging receptor SCARF1<sup>16</sup>, and soluble bridging protein, milk fat globule epidermal growth factor 8 (MFG-E8), that recognizes phosphatidylserine on ACs<sup>17,18</sup>. However, while these whole-body knockout studies establish a role for defective efferocytosis in autoimmune-like phenotypes, it remains unclear whether myeloid-specific defects alone can drive systemic autoimmune responses. Open questions also remain about whether the immunogenic autoantigens produced due to insufficient efferocytosis are the sole cause of increased autoimmunity, or if efferocytosis of ACs directly impacts the ability of macrophages to activate T cells and potentially amplify autoimmune responses. Additionally, it has not been established if enhancing macrophage efferocytosis or modulating macrophage responses to AC engulfment can be protective in autoimmune-like disorders.

We have previously identified, via a genome-wide CRISPR screening, that WDFY3 is required for both the engulfment and the subsequent lysosomal acidification and degradation of ACs by macrophages<sup>19</sup>. Here, using myeloid-specific *Wdfy3* knockout and ectopic WDFY3 overexpression in mice, along with WDFY3 knockdown in human macrophages, we show that myeloid *Wdfy3* loss drives autoimmunity, whereas overexpression enhances efferocytosis and confers protection. These effects are observed in both young mice with increased AC burden and middle-aged mice that develop spontaneous autoreactivity. Mechanistically, WDFY3 promotes efferocytosis and limits CD4<sup>+</sup> T cell activation by suppressing MHC-II-mediated antigen presentation and cytokine dysregulation. Thus, beyond clearing ACs, macrophages actively respond to efferocytosis by modulating immune functions such as cytokine secretion and T cell activation, a process regulated by WDFY3. Our findings position WDFY3 as a protective factor against autoimmune pathogenesis linked to impaired efferocytosis and highlight the opportunities in targeting macrophage efferocytosis to mitigate autoimmune disorders and age-associated chronic inflammation.

## Results

### Myeloid knockout of *Wdfy3* exacerbates autoimmunity induced by systemic AC injections in young mice and spontaneous autoreactivity in middle-aged mice

Given our previous findings demonstrating the importance of WDFY3 in regulating multiple steps of the efferocytic clearance of ACs<sup>19</sup>, we set out to determine the pathological consequence of impaired efferocytosis in mice with myeloid knockout of *Wdfy3*. Delayed clearance of exogenously injected ACs leads to progressive development of autoantibodies and autoimmune disorders<sup>14</sup>. Using a similar approach, we aimed to determine whether myeloid-specific knockout of *Wdfy3* will exacerbate autoimmune responses induced by increasing the burden of ACs through systemic injections.

We backcrossed *Wdfy3*<sup>fl/fl</sup> mice<sup>20</sup> generated by insertion of two *loxP* sites flanking exon 5 to mice on a C57BL/6J background for nine generations. Myeloid-specific *Wdfy3* null mice were obtained by breeding *Wdfy3*<sup>fl/fl</sup> mice with *LysMCre* mice for Cre-mediated recombination in the myeloid cell lineage<sup>21</sup>, including monocytes, mature macrophages, and granulocytes, i.e. *LysMCre*<sup>+/+</sup>*Wdfy3*<sup>fl/fl</sup> mice (Cre<sup>+</sup>), while using *LysMCre*<sup>-/-</sup>*Wdfy3*<sup>fl/fl</sup> littermates (Cre<sup>-</sup>) as the controls (as illustrated in Fig. 1a); and the loss of WDFY3 protein and impaired efferocytosis in Cre<sup>+</sup> macrophages were established in our previous study<sup>19</sup>. We further confirmed that *LysMCre*-mediated *Wdfy3* knockout is specific to BMDMs, as it did not affect WDFY3 protein expression in BM-derived dendritic cells (BMDC), nor did it alter BMDC

differentiation or efferocytosis (Supplementary Fig. 1). Beginning at 8–10 weeks of age, Cre<sup>-</sup> and Cre<sup>+</sup> mice were injected with UV irradiation-induced apoptotic murine thymocytes over an 8-week period (Fig. 1a for study design) and examined for markers of organ dysfunction (Fig. 1b, c), serum autoantibodies (Fig. 1d, e), and kidney histology and immune complex deposition (Fig. 1f–i). Markers of liver and kidney dysfunction, including serum alanine aminotransferase (ALT) and creatinine (Fig. 1b, c), did not differ between Cre<sup>-</sup> and Cre<sup>+</sup> mice with AC injections. Cre<sup>+</sup> mice that received AC injections showed higher serum antinuclear antibodies (ANA) total Ig compared to Cre<sup>-</sup> mice with AC injections, indicating increased autoantigen availability in Cre<sup>+</sup> mice (Fig. 1d). Anti-dsDNA total Ig (Fig. 1e) did not differ across genotypes. Cre<sup>+</sup> mice exhibited more severe histological features of glomerulonephritis in response to AC injections, including enlarged area (Fig. 1f) and increased glomerular mesangial hypercellularity (Fig. 1g). Furthermore, Cre<sup>+</sup> mice displayed increased C1q and IgG deposition in the glomerular mesangium compared to Cre<sup>-</sup> mice with AC injections (Fig. 1h, i). These same parameters assessed in Fig. 1 were also examined in Cre<sup>-</sup> and Cre<sup>+</sup> mice without receiving AC injections (Supplementary Fig. 2). In these mice without AC burden, ALT, ANA total Ig, anti-dsDNA total Ig, glomerular size and immune complex deposition in the kidney remained low and did not differ between Cre<sup>-</sup> and Cre<sup>+</sup> mice, suggesting that myeloid-specific knockout of *Wdfy3* alone was not sufficient to induce autoimmune phenotypes in these mice. To directly assess the extent of ANA induction following systemic AC injections, we visualized data from mice with and without AC injections side-by-side (Supplementary Fig. 3). ANA total Ig levels increased approximately 2-fold (Supplementary Fig. 3a), while ANA IgG levels showed a more modest increase (Supplementary Fig. 3b), indicating a mild autoimmune response. These relatively modest pathological changes induced by systemic AC injections were consistent with previous studies in mice on a B6 genetic background<sup>22</sup>, which exhibited milder phenotypes compared to more susceptible strains. Myeloid knockout of *Wdfy3* worsened serum ANA total Ig and kidney immune complex deposition, but not ANA IgG, likely due to the limited susceptibility of this genetic background to more severe systemic responses.

The kidney immune complex deposition and nephritis-like phenotype were unlikely due to the direct effects of intrarenal AC accumulation, since the injected ACs mostly accumulated in the spleen (Supplementary Fig. 4), underscoring the role of spleen in the autoimmune cascade. The increased autoimmune phenotypes in AC-injected Cre<sup>+</sup> mice are also unlikely to be due to changes in macrophage development or expression of efferocytic receptors, since the percentage of spleen and liver macrophages and their expression of MerTK, AXL, and TIM4 (by flow cytometry) and CD68<sup>+</sup> macrophage area (by immunofluorescence staining) were comparable between Cre<sup>-</sup> and Cre<sup>+</sup> mice (Supplementary Fig. 5).

Autoinflammatory and autoimmune responses progress with age, advancing from autoreactivity to autoimmunity, when immune dysregulation, impaired efferocytosis, and chronic inflammation disrupt tolerance and amplify autoreactive T and B cell activities<sup>23</sup>. To explore whether myeloid knockout of *Wdfy3* accelerates age-associated autoimmunity, we observed mice at midlife (52–60-week-old). Consistent with what we have published in young mice<sup>19</sup>, BMDMs of middle-aged Cre<sup>+</sup> mice showed a complete loss of WDFY3 protein (Supplementary Fig. 6b) and impaired efferocytosis, including engulfment and acidification of the engulfed ACs, compared to Cre<sup>-</sup> controls (Supplementary Fig. 6c). Middle-aged Cre<sup>+</sup> mice also showed increased spleen and kidney weight (Supplementary Fig. 6d) and increased serum ALT, a marker of hepatocyte death, compared to Cre<sup>-</sup> controls (Supplementary Fig. 6e). Creatinine was comparable between Cre<sup>-</sup> and Cre<sup>+</sup> mice (Supplementary Fig. 6f), suggesting no kidney dysfunction in these mice despite histological changes at this stage. Serum ANA total Ig was increased

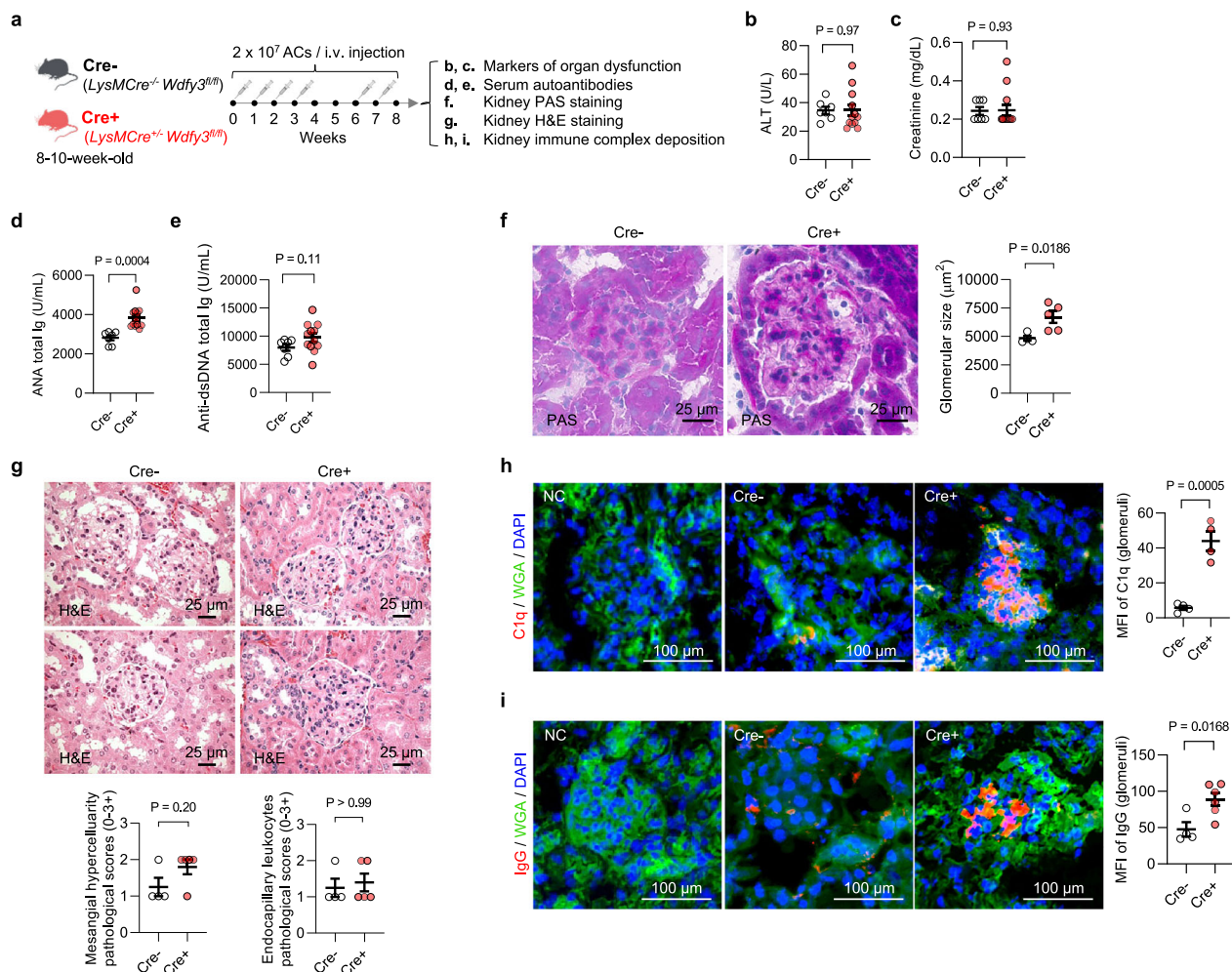


**Fig. 1 | Myeloid knockout of *Wdfy3* exacerbates autoimmune responses in mice receiving systemic apoptotic cell injections. a** Schematics of study design. Mice with *LysMCre*-mediated myeloid-specific knockout of *Wdfy3* ( $Cre^+$ , *LysMCre<sup>+</sup>Wdfy3<sup>fl/fl</sup>*) and the respective controls ( $Cre^-$ , *LysMCre<sup>+</sup>Wdfy3<sup>fl/fl</sup>*) were bred, and age- and sex-matched littermates were used for experiments. To increase the burden of apoptotic cells (AC), murine thymocytes underwent UV irradiation to induce apoptosis. Subsequently, ACs were injected intravenously via the tail vein according to the timeline illustrated. Serum samples were collected to determine markers of organ dysfunction and autoantibodies. Kidneys were dissected and sectioned for periodic acid-Schiff (PAS), H&E, and immunofluorescence staining. **b** Serum alanine transaminase (ALT), a marker of hepatocyte death.  $n = 7$   $Cre^-$  vs 12  $Cre^+$  mice. **c** Serum creatinine, a marker of kidney dysfunction.  $n = 7$   $Cre^-$  vs 13  $Cre^+$  mice. **d** Serum anti-nuclear antibodies (ANA) total Ig.  $n = 7$   $Cre^-$  vs 12  $Cre^+$  mice.

**e** Serum anti-dsDNA total Ig.  $n = 7$   $Cre^-$  vs 12  $Cre^+$  mice. **f** PAS staining of kidney sections highlight glomerular basement membrane for the quantification of glomerular size.  $n = 4$   $Cre^-$  vs 5  $Cre^+$  mice. Scale bar = 25  $\mu$ m. **g** H&E staining of kidney sections was performed to assess mesangial hypercellularity (left) and endocapillary hypercellularity/leukocyte infiltration (right).  $n = 4$   $Cre^-$  vs 5  $Cre^+$  mice. Scale bar = 25  $\mu$ m. **h, i** Immunofluorescence staining of kidney sections using anti-C1q and anti-IgG antibodies (red) and wheat germ agglutinin (WGA, green) to outline glomeruli. Mean fluorescent intensity (MFI) of C1q (**h**) and IgG (**i**) in the glomeruli area were quantified.  $n = 4$   $Cre^-$  vs 4  $Cre^+$  mice (**h**);  $n = 4$   $Cre^-$  vs 6  $Cre^+$  mice (**i**). NC negative control. Scale bar = 100  $\mu$ m. Data are shown as mean  $\pm$  standard error of the mean (SEM). A two-tailed Student's *t*-test was applied to all data, except for (**g**), where a two-tailed Mann–Whitney *U* test was performed.

in  $Cre^+$  middle-aged mice (Supplementary Fig. 6g), together with increased glomerular size (Supplementary Fig. 6i) and C1q and IgG immune complex deposition in the glomeruli (Supplementary Fig. 6j, k). Anti-dsDNA total Ig (Supplementary Fig. 6h) were not different between middle-aged  $Cre^-$  and  $Cre^+$  mice. These middle-aged mice also did not demonstrate overt lupus-like pathological changes in the kidney, spleen, liver, or skin, other than mild kidney mesangial hypercellularity and sclerosis; several mice also had mild-to-modest hepatic steatosis (Supplementary Data 1). These results suggest that, while still preclinical, myeloid knockout of *Wdfy3* accelerates age-associated autoreactivity in middle-aged mice. This phenotype, emerging without external triggers, likely results from defective efferocytosis and age-associated increases in cell death, leading to self-antigen exposure, ANA production, and immune complex-mediated glomerular enlargement.

### Myeloid knockout of *Wdfy3* exacerbates autoimmunity via efferocytosis-dependent and macrophage-intrinsic mechanisms, including enhanced antigen presentation and IL-1 $\beta$ secretion

It remains unclear whether autoimmunity is solely triggered by increased immunogenic autoantigens from dead cells because of impaired clearance, or if the cell-intrinsic effects within macrophages triggered by AC engulfment directly impact macrophages' ability to activate T cells and potentially amplify autoimmune responses.

While myeloid knockout of *Wdfy3* was not sufficient to drive autoimmune-like disorders in young mice without an increased AC burden, we found that young mice with myeloid knockout of *Wdfy3* showed increased T cell activation (Fig. 2a for study design). Specifically,  $Cre^+$  mice had an increased percentage of CD44<sup>hi</sup>CD62L<sup>lo</sup> activated T cells in CD4<sup>+</sup> T cells, though not CD8<sup>+</sup> T cells, in the blood and



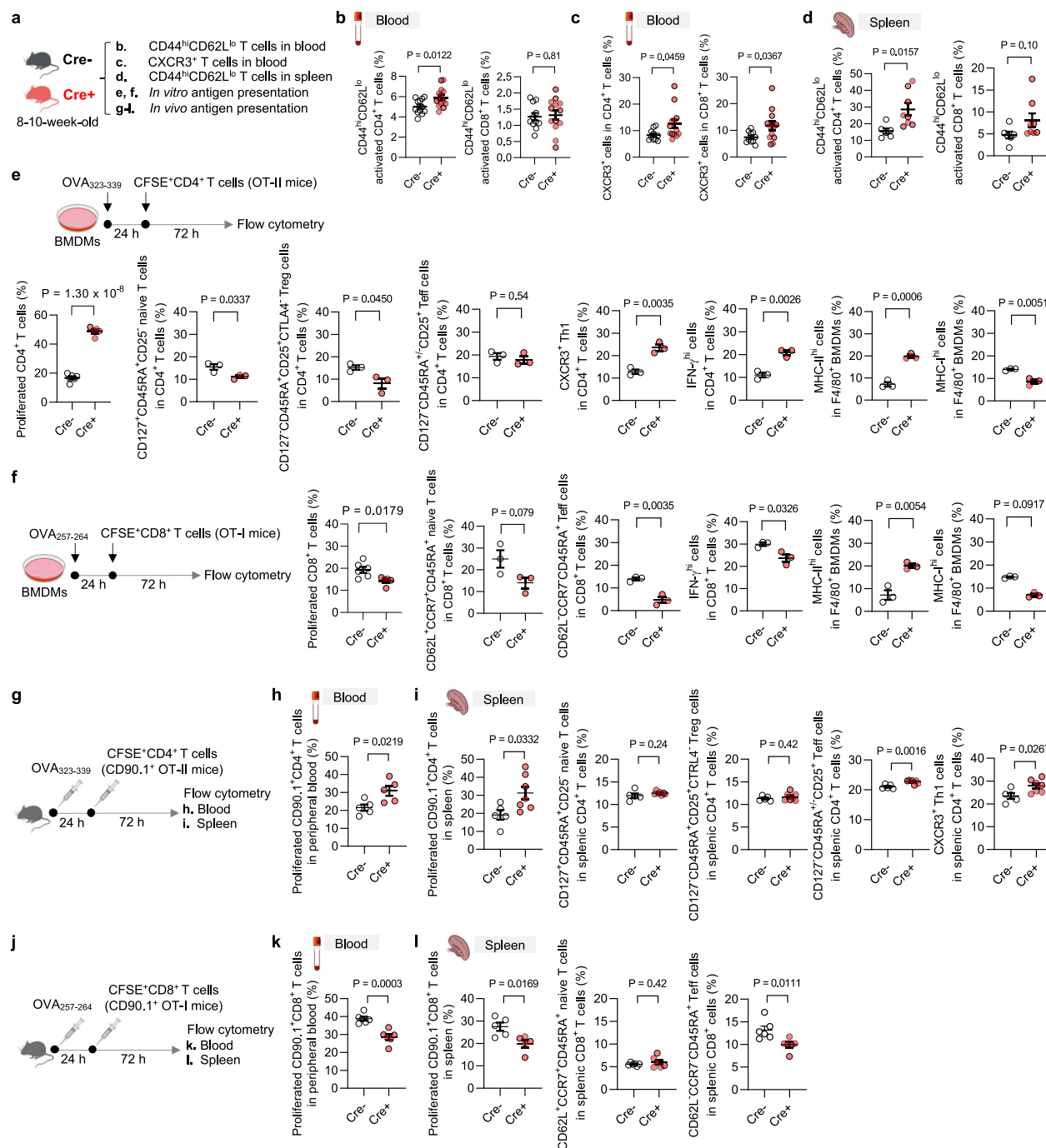


**Fig. 2 | Myeloid knockout of *Wdfy3* augments CD4<sup>+</sup> T cell activation by promoting MHC-II-mediated antigen presentation.** **a** Schematics of study design. Cre<sup>-</sup> and Cre<sup>+</sup> littermates were used to assess T cell activation. **b** The percentage of CD44<sup>high</sup>CD62L<sup>low</sup> activated T cells in CD4<sup>+</sup> and CD8<sup>+</sup> T cells in the blood.  $n = 12$  Cre<sup>-</sup> vs 14 Cre<sup>+</sup> mice and  $n = 11$  Cre<sup>-</sup> vs 13 Cre<sup>+</sup> mice, respectively. **c** The percentage of CXCR3<sup>+</sup> activated T cells in CD4<sup>+</sup> and CD8<sup>+</sup> T cells in the blood.  $n = 10$  Cre<sup>-</sup> vs 13 Cre<sup>+</sup> mice. **d** The percentage of CD44<sup>high</sup>CD62L<sup>low</sup> activated T cells in splenic CD4<sup>+</sup> and CD8<sup>+</sup> T cells.  $n = 6$  Cre<sup>-</sup> vs 8 Cre<sup>+</sup> mice. **e, f** *In vitro* antigen presentation assay. BMDMs were pre-treated with synthetic ovalbumin (OVA) for 24 h, followed by incubating with splenic T cells isolated from OT-II or OT-I transgenic mice for 72 h to assess OVA<sub>323-339</sub> or OVA<sub>257-264</sub>-specific activation of CD4<sup>+</sup> T cells (OT-II mice) or CD8<sup>+</sup> T cells (OT-I mice) that recognize OVA peptide residues when presented by the MHC-II or MHC-I molecules, respectively. The OT-II or OT-I mouse T cells were pre-labeled by carboxy-fluorescein succinimidyl ester (CFSE) to monitor the

dilution of CFSE signal in daughter cells as T cells divide.  $n = 6$  Cre<sup>-</sup> vs 5 Cre<sup>+</sup> mice. Effector T cell differentiation was assessed using a set of markers as indicated in the figures.  $n = 3$  Cre<sup>-</sup> vs 3 Cre<sup>+</sup> mice. **g–i** *In vivo* antigen presentation assay. **g–i** Mice were immunized with OVA<sub>323-339</sub> for 24 h before the injection of CFSE-labeled splenic CD4<sup>+</sup> T cells from CD90.1<sup>+</sup> OT-II mice. 72 h after injection, CFSE dilution in CD4<sup>+</sup>CD90.1<sup>+</sup> blood and splenic T cells, and splenic T cell activation were assessed.  $n = 5$  Cre<sup>-</sup> vs 5 Cre<sup>+</sup> mice for blood, and  $n = 5$  Cre<sup>-</sup> vs 7 Cre<sup>+</sup> mice for spleen. **j–l** Mice were immunized with OVA<sub>257-264</sub> for 24 h before the injection of CFSE-labeled splenic CD8<sup>+</sup> T cells from CD90.1<sup>+</sup> OT-I mice. 72 h after injection, CFSE dilution in CD8<sup>+</sup>CD90.1<sup>+</sup> blood and splenic T cells, and splenic T cell activation were assessed. For blood,  $n = 6$  Cre<sup>-</sup> vs 6 Cre<sup>+</sup> mice; for spleen,  $n = 5$  Cre<sup>-</sup> vs 5 Cre<sup>+</sup> mice (proliferation) and 6 Cre<sup>-</sup> vs 6 Cre<sup>+</sup> mice (T cell subsets). Data are shown as mean  $\pm$  SEM. A two-tailed Student's *t*-test was applied to all data.

spleen (Fig. 2b, d, Supplementary Fig. 7a for gating strategies). CXCR3, a chemokine receptor that is highly expressed on effector T cells<sup>24</sup>, was modestly increased in CD4<sup>+</sup> and CD8<sup>+</sup> T cells in the blood of Cre<sup>+</sup> mice (Fig. 2c, Supplementary Fig. 7a for gating strategies).

T cells are activated when their receptors recognize antigens presented by antigen-presenting cells, such as macrophages, DCs, and B cells, and receive additional signals from cytokines<sup>25–27</sup>. To determine if macrophage WDFY3 directly regulates antigen presentation capacity by macrophages via cell intrinsic mechanisms, we performed a standard antigen presentation assay using soluble antigens, which require the interaction of the MHC complex on ovalbumin (OVA)-treated macrophages with T cells isolated from OT-II or OT-I transgenic mice (Fig. 2e, f, Supplementary Fig. 7b–d for gating strategies). The OT-II transgenic mice express mouse T cell receptors designed to specifically recognize OVA peptide residues 323–339 (OVA<sub>323–339</sub>), when presented to CD4<sup>+</sup> T cells by the MHC-II molecule, whereas OT-I transgenic mice express mouse T cell receptors designed to recognize OVA peptide residues 257–264 (OVA<sub>257–264</sub>), when presented to the CD8<sup>+</sup> T cells by the MHC-I molecule. T cells were labeled with carboxy-fluorescein succinimidyl ester (CFSE). CFSE dilution indicates T cell proliferation. We found that knockout of *Wdfy3* in macrophages led to increased MHC-II-mediated antigen presentation to CD4<sup>+</sup> T cells, leading to increased T cell expansion, decreased regulatory T cells (Tregs) and increased Th1 cells, as well as increased intracellular IFN- $\gamma$  expression (Fig. 2e). In contrast, Cre<sup>+</sup> BMDMs showed decreased MHC-I-mediated antigen presentation to CD8<sup>+</sup> T cells (Fig. 2f). Mechanistically, Cre<sup>+</sup> BMDMs showed a higher proportion of MHC-I<sup>hi</sup> and a lower proportion of MHC-I<sup>hi</sup> cells compared to Cre<sup>−</sup> BMDMs (Fig. 2e, f).

To confirm our findings in vivo, we immunized Cre<sup>+</sup> mice and their control counterparts with OVA<sub>323–339</sub>, followed by an adoptive transplantation of CD4<sup>+</sup> T cells from CD90.1<sup>+</sup> OT-II mice<sup>25</sup>, which specifically recognize OVA-MHC-II complexes. The distinction of donor T cells from the recipient's T cells relies on the expression of CD90.1, a surface marker that is unique to the donor T cells, while the recipient mice express CD90.2<sup>25</sup> (Schematics in Fig. 2g, j). In Cre<sup>+</sup> mice, there was a significant CFSE dilution and increased effector T cells in CD4<sup>+</sup>CD90.1<sup>+</sup>OT-II T cells in the blood and spleen (Fig. 2h, i), indicating enhanced T cell expansion and activation. In contrast, knockout of *Wdfy3* in macrophages resulted in decrease in MHC-I-mediated antigen presentation to CD8<sup>+</sup> T cells in vivo (Fig. 2k, l), consistent with the results in vitro.

We next determined if T cell activation is associated with increased inflammatory cytokine production at systemic levels and the cellular mechanisms (Fig. 3a for schematic design). We used a 26-Plex ProcartaPlex mouse cytokine and chemokine panel, which includes cytokines produced by activated T cells or those that instruct T cell activation (Supplementary Fig. 8). Among all the cytokines/chemokines tested in the panel, only IL-18 was increased in the serum of Cre<sup>+</sup> mice (Fig. 3b). IL-18, together with IL-1 $\beta$  and IL-1 $\alpha$ , are pro-inflammatory cytokines in the IL-1 family<sup>28,29</sup>. Their secretion, especially the secretion of IL-1 $\beta$  and IL-18, is regulated by inflammasomes which are multi-protein complexes containing sensor proteins, adaptor protein and caspase-1<sup>28,29</sup>. IL-1 $\beta$  and IL-18 are the direct indicator of inflammasome activation and caspase-1 is a key effector enzyme involved in the cleavage and activation of pro-IL-1 $\beta$  and pro-IL-18. We therefore examined whether the knockout *Wdfy3* in macrophages affects inflammasome activation. Indeed, F4/80<sup>+</sup> splenic macrophages of Cre<sup>+</sup> mice showed increased pro-IL-1 $\beta$  protein expression (Fig. 3c) and caspase-1 cleavage (Fig. 3d), suggesting enhanced priming and activation of the inflammasome in these mice.

To investigate whether *Wdfy3* knockout in macrophages can exacerbate IL-1 $\beta$  secretion in the context of efferocytosis, we used an in vitro model in which BMDMs were co-incubated with ACs for 8 h, followed by measurement of IL-1 $\beta$  levels in the culture media. Efferocytosis induced modest secretion of IL-1 $\beta$ , which was further

enhanced by *Wdfy3* knockout (Fig. 3e). In BMDMs that had engulfed ACs, Cre<sup>+</sup> cells showed higher expression of ASC (apoptosis-associated speck-like protein containing a CARD) by immunostaining compared to Cre<sup>−</sup> cells; however, ASC specks, hallmarks of inflammasome activation, were not observed under these experimental conditions (Fig. 3f). In human monocyte-derived macrophages (HMDM), siRNA-mediated *WDFY3* knockdown enhanced caspase-1 cleavage in response to ACs, as well as to LPS and ATP, which activate the NLRP3 inflammasome (Fig. 3g). Together, these in vitro experiments suggest that while efferocytosis is widely recognized for inducing anti-inflammatory cytokines, it can also trigger modest secretion of IL-1 $\beta$ . This effect is amplified by *Wdfy3* deficiency through canonical inflammasome components, although full inflammasome activation likely require additional stimuli<sup>30</sup>.

IL-1 $\beta$  is known to enhance antigen-primed CD4<sup>+</sup> T-cell activation<sup>31</sup>. To directly test how efferocyte and T cell interaction affects T cell activation, we co-incubated BMDMs with ACs to induce efferocytosis, followed by co-culture with CD4<sup>+</sup> T cells and determined T cell differentiation, based on a previously published protocol with modification<sup>32</sup>. Compared to Cre<sup>−</sup> BMDMs, efferocytic Cre<sup>+</sup> BMDMs led to decreased CD127<sup>+</sup>CD45RA<sup>+</sup>CD25<sup>+</sup>CTLA4<sup>−</sup> Tregs and increased CD28<sup>+</sup>CCR4<sup>+</sup> Th22 cells (Fig. 3h, Supplementary Fig. 7b for gating strategies). Reduced Tregs impair immune suppression, allowing excessive T cell activation, while increased Th22 cells amplify inflammation in tissue-specific autoimmune diseases<sup>33</sup>, suggesting a heightened risk of T cell activation and uncontrolled inflammation.

Taken together, myeloid *Wdfy3* knockout leads to increased CD4<sup>+</sup> T cell activation likely via efferocytosis-dependent and macrophage-intrinsic mechanisms by enhancing antigen presentation capacity and IL-1 $\beta$  secretion.

### Overexpression of WDFY3 enhances macrophage efferocytosis in vitro and in vivo

Given how the loss of WDFY3 diminishes efferocytosis and promotes autoimmunity, we next investigated whether increasing expression levels of WDFY3 could enhance efferocytosis and mitigate autoimmunity (Fig. 4a for schematics). Mice for overexpressing human *WDFY3* were generated by knocking the construct, *loxP-STOP-loxP-3xFLAG-hWDFY3* cDNA, into the *Rosa26* locus (*Rosa26*<sup>*loxP-STOP-loxP-3xFLAG-hWDFY3*</sup> cDNA<sup>34</sup>). To achieve constitutive overexpression, male mice carrying the floxed alleles were crossed with female carrier of *HprtCre*<sup>35</sup>, a Cre-deleter strain with 100% Cre-mediated recombination in oocytes to generate heritable deletion of *loxP-STOP-loxP* cassette (*Rosa26*<sup>*3xFLAG-hWDFY3*</sup>). *Rosa26*<sup>*3xFLAG-hWDFY3*</sup> mice were interbred to generate homozygotes knock-in (KI) mice (hWDFY3<sup>KI/KI</sup>) and wildtype littermate controls (Ctrl) and were maintained on a mixed background (C57BL/6  $\times$  129/SvEv).

BMDMs from hWDFY3<sup>KI/KI</sup> mice show higher levels of WDFY3 expression by Western blotting (Fig. 4b), accompanied by higher engulfment capacity compared to their control counterparts (Fig. 4c). Consistent with our loss-of-function studies showing impaired LC3 lipidation and lysosomal acidification of engulfed ACs in macrophages of Cre<sup>+</sup> mice<sup>19</sup>, BMDMs of WDFY3-overexpressing mice had a modest increase in the percentage of engulfed ACs that were also acidified (Fig. 4c). This was accompanied by increased LC3 lipidation (Fig. 4d), which aids in phagosome-lysosome fusion and the subsequent lysosomal acidification<sup>36</sup>. This modest increase suggests that the enhanced engulfment of cargo is associated with efficient degradation. We also confirmed enhanced efferocytosis in peritoneal macrophages (PM) of WDFY3-overexpressing mice (Fig. 4e).

We further validated efferocytosis in mice using two in vivo assays: thymus efferocytosis and PM efferocytosis<sup>19</sup>. The in vivo thymus efferocytosis assay involved injecting dexamethasone intraperitoneally into Ctrl and hWDFY3<sup>KI/KI</sup> mice to induce thymocyte apoptosis (Fig. 4f), as the thymus is particularly sensitive to dexamethasone-

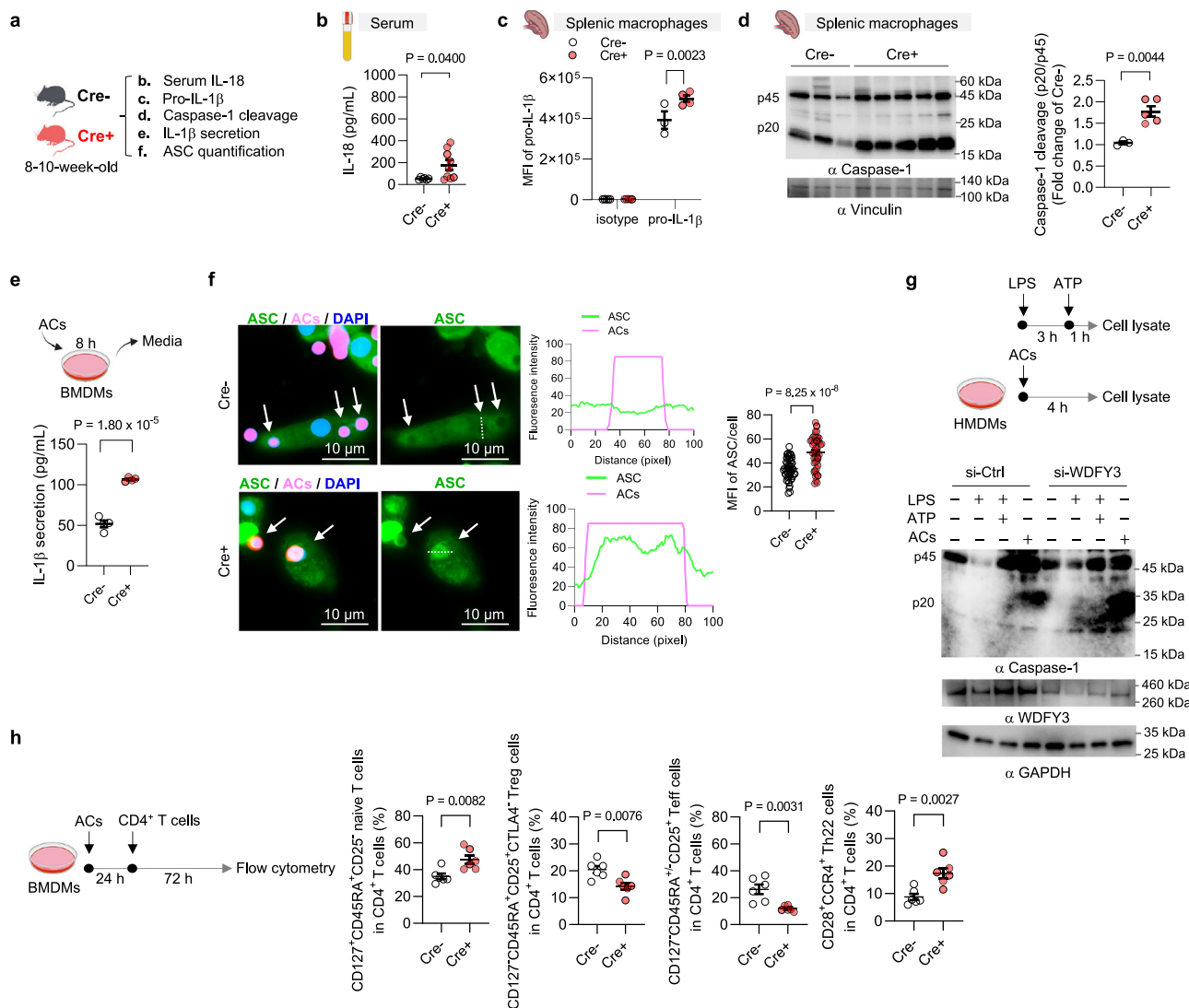


**Fig. 3 | Myeloid knockout of *Wdfy3* augments inflammasome activation and efferocyte-T cell interaction.** **a** Schematics of study design. Cre<sup>-</sup> and Cre<sup>+</sup> littermates were used to assess inflammasome activation. **b** Serum IL-18. **c** The expression of pro-IL-1β in F4/80<sup>+</sup> splenic macrophages assessed by flow cytometry. MFI, median fluorescence intensity. **d** Analysis of intracellular caspase-1 cleavage in F4/80<sup>+</sup> splenic macrophages by Western blotting. The intensity of the active form of caspase-1, p20, was quantified and compared to the intensity of the pro-caspase-1 (p45). The ratio of p20 intensity to p45 intensity was calculated, and this ratio was normalized to the control group (Cre<sup>-</sup>), which was assigned a value of 1.0 for standardization. **e** BMDMs were co-incubated with ACs at a 5:1 AC-to-BMDM ratio for 8 h. Culture media were collected to determine IL-1β by ELISA. **f** Quantification of ASC expression in efferocytes. White arrows indicate ACs engulfed by BMDMs. The dashed line traverses the engulfed AC, indicating the axis along which fluorescence intensity of ASC and the engulfed AC were plotted to illustrate increased ASC signals surrounding the engulfed AC. The mean fluorescence intensity (MFI) of ASC

per cell was quantified in BMDMs that had engulfed ACs.  $n = 50$  cells from 5 Cre<sup>-</sup> mice vs 44 cells from 5 Cre<sup>+</sup> mice. Scale bar = 10 μm. **g** Human peripheral blood monocytes were differentiated into macrophages (HMDM) followed by transfection of non-targeting control siRNA (si-Ctrl) or siRNAs targeting *WDFY3* (si-WDFY3). At day 7, HMDMs were primed with 20 ng/mL lipopolysaccharide (LPS) for 3 h and then treated with 2 mM ATP for an additional 1 h to induce inflammasome activation. To assess if AC engulfment induces caspase-1 cleavage in the efferocytes, we co-incubated HMDMs with ACs for 4 h at a 5:1 AC-to-HMDM ratio. Unbound ACs were washed away. HMDMs were harvested to determine caspase-1 cleavage by Western blotting. The representative blot from three technical replicates was shown. **h** Efferocyte-T cell interaction. BMDMs were co-incubated with ACs for 24 h and then removed by washing, followed by co-culture with CD4<sup>+</sup> splenic T cells for 72 h to assess efferocyte-mediated activation of CD4<sup>+</sup> T cells.  $n = 6$  Cre<sup>-</sup> vs 6 Cre<sup>+</sup> mice. Data are shown as mean ± SEM. A two-tailed Student's *t*-test was applied to all data, except for Fig. 3c, where a two-way ANOVA was performed, followed by Sidak's post hoc test to adjust for multiple comparisons.

induced apoptosis<sup>37</sup>. After 18 h, we assessed thymus weight and cellularity (Fig. 4g, h). Compared to the Ctrl mice, hWDFY3<sup>KI/KI</sup> mice showed lower thymus weights and decreased cellularity (Fig. 4g, h), indicating enhanced efferocytic clearance of apoptotic thymocytes. Consistently, thymi from hWDFY3<sup>KI/KI</sup> mice also contained fewer Annexin V<sup>+</sup> cells (Fig. 4i). We next assessed in situ efferocytosis using TUNEL staining on thymus sections to calculate the ratio of TUNEL<sup>+</sup> cells associated with CD68<sup>+</sup> macrophages and free TUNEL<sup>+</sup> cells not in

proximity to macrophages (Fig. 4j). The data showed an increased ratio of macrophage-associated AC: free AC in hWDFY3<sup>KI/KI</sup> mice, indicating increased efferocytosis in the thymus. We further confirmed our findings by assessing PM efferocytosis in vivo. Peritoneal exudate was collected 15 min after injecting TAMRA-labeled ACs<sup>19</sup>. PMs from hWDFY3<sup>KI/KI</sup> mice showed an increased percentage of TAMRA-labeled F4/80<sup>+</sup> macrophages, indicating enhanced efferocytotic capacity in the hWDFY3<sup>KI/KI</sup> mice (Fig. 4k).

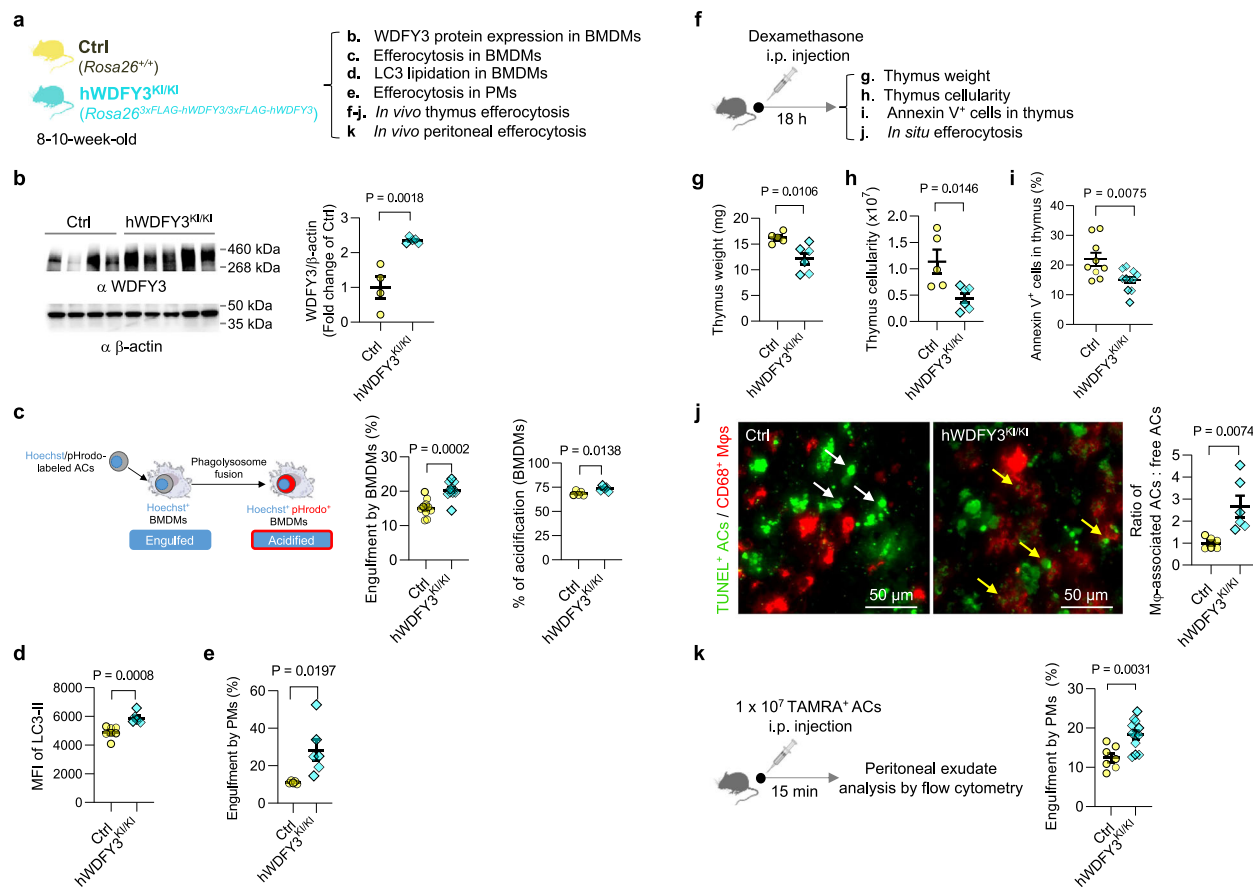


**Fig. 4 | Overexpression of *WDFY3* enhances efferocytosis in vitro in macrophages and in vivo in mice.** **a** Schematics of experimental design. Mice with ectopic overexpression of human *WDFY3* were generated by knock-in (KI) of the construct, i.e., cDNA sequence encoding 3× FLAG tag that is fused to human *WDFY3* cDNA preceded by a STOP cassette flanked by *loxP* sites, into the *Rosa26* locus (*Rosa26<sup>cre-loxP-STOP-loxP-3xFLAG-hWDFY3</sup>*). Constitutive overexpression was achieved by breeding male mice carrying the floxed allele with female *HprtCre* to generate heritable deletion of the *loxP-STOP-loxP* cassette (*Rosa26<sup>3xFLAG-hWDFY3</sup>*). *Rosa26<sup>3xFLAG-hWDFY3</sup>* mice were interbred to generate homozygotes *Rosa26<sup>3xFLAG-hWDFY3</sup>* (*hWDFY3<sup>KI/KI</sup>*) and wildtype littermate controls *Rosa26<sup>+/+</sup>* (Ctrl). **b** Validation of overexpression of *WDFY3* in BMDMs by Western blotting. **c** BMDMs were incubated with ACs labeled by Hoechst, which stains DNA and is pH-insensitive, and pHrodo-Red, which is pH-sensitive and fluoresces only in an acidified environment in the phagolysosome. The percentage of Hoechst<sup>+</sup> BMDMs indicates engulfment. **d** BMDMs were incubated with Hoechst-labeled ACs to allow for efferocytosis. After removal of unbound ACs, BMDMs were collected and treated with digitonin to remove non-membrane bound LC3, and then immunostained for LC3 that is lipidated and membrane-bound, i.e. LC3-II. LC3-II staining was then quantified by flow cytometry for BMDMs that had engulfed Hoechst-labeled ACs. MFI, median fluorescence intensity. **e** Peritoneal exudates were seeded and nonadherent

cells were removed. The remaining peritoneal macrophages (PM) were cultured for 18 h and then incubated with Hoechst-labeled ACs to allow for efferocytosis. After 1 h, unbound ACs were washed away, and PMs were harvested to quantify the % of Hoechst<sup>+</sup> PMs by flow cytometry. **f** Schematic of experimental design for in vivo thymus efferocytosis. Mice were injected intraperitoneally with dexamethasone to induce thymocyte apoptosis. 18 h after injection, thymi were dissected for assessment of the following parameters. **g** Thymus weight. **h** Total number of cells per thymus. **i** The percentage of Annexin V<sup>+</sup> cells per thymus. **j** In situ efferocytosis. Thymic sections were stained with TUNEL for ACs (green), and CD68 for macrophages (red). The ratio of macrophage-associated TUNEL<sup>+</sup> cells vs. free TUNEL<sup>+</sup> cells was quantified to assess in situ efferocytosis in the thymus. The white and yellow arrows highlight free and macrophage-associated TUNEL<sup>+</sup> cells, respectively. Lower weight and cellularity, lower percentage of Annexin V<sup>+</sup> cells, and higher in situ efferocytosis indicate enhanced efferocytosis capacity. **k** In vivo PM efferocytosis assay.  $1 \times 10^7$  TAMRA<sup>+</sup> ACs were injected intraperitoneally, and peritoneal exudates were collected after 15 min. After blocking with CD16/32, peritoneal cells were stained with F4/80 antibody to label PMs and the percentage of TAMRA<sup>+</sup> PMs was determined by flow cytometry. Data are shown as mean ± SEM. A two-tailed Student's *t*-test was applied to all data.

### Overexpression of *WDFY3* attenuates autoimmunity induced by systemic AC injections in young mice and autoreactivity in middle-aged mice

After confirming the enhanced efferocytic capacity in macrophages overexpressing *WDFY3*, we asked whether *WDFY3* overexpression in mice protects against autoimmunity. We challenged *hWDFY3<sup>KI/KI</sup>* mice with repeated injections of ACs as described for loss-of-function studies in Fig. 1 (also illustrated in Fig. 5a), and assessed markers of organ dysfunction, circulating autoantibodies, kidney histology and immune complex deposition (Fig. 5). Markers of organ dysfunction remained

low and comparable between Ctrl and *hWDFY3<sup>KI/KI</sup>* mice (Fig. 5b, c). However, compared to Ctrl mice, *hWDFY3<sup>KI/KI</sup>* mice showed lower levels of ANA total Ig and anti-dsDNA total Ig (Fig. 5d, e), smaller glomeruli (Fig. 5f), and reduced C1q and IgG deposition in the kidney (Fig. 5g, h), indicating a protective effect from AC injections. Compared to Ctrl and *hWDFY3<sup>KI/KI</sup>* without AC injections, ANA total Ig and anti-dsDNA total Ig levels were increased approximately 2-fold following AC injections (Supplementary Fig. 9 and Fig. 5d, e).

The protective effects of *WDFY3* overexpression also extended to middle-aged mice without AC injections (Supplementary Fig. 10a for



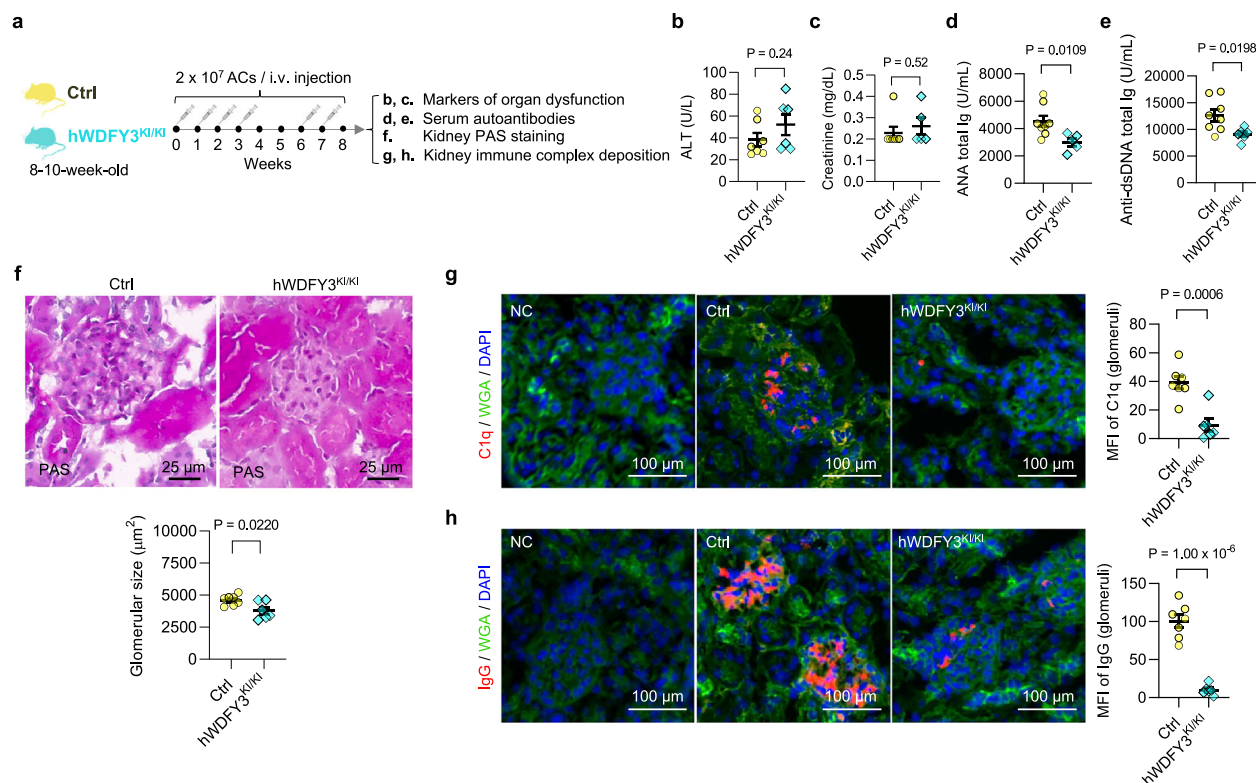


**Fig. 5 | Overexpression of *WDFY3* mitigates autoimmune responses in mice receiving systemic AC injections.** **a** Schematics of study design. Age- and sex-matched Ctrl and hWDFY3<sup>KI/KI</sup> littermates were used for experiments. ACs were prepared and injected as illustrated and as described in Fig. 1a. Serum samples were collected to determine markers of organ dysfunction and autoantibodies. Kidneys were dissected and sectioned for PAS and immunofluorescence staining. **b** Serum ALT.  $n = 7$  Ctrl vs 6 hWDFY3<sup>KI/KI</sup> mice. **c** Serum creatinine.  $n = 7$  Ctrl vs 5 hWDFY3<sup>KI/KI</sup> mice. **d** Serum ANA total Ig.  $n = 8$  Ctrl vs 5 hWDFY3<sup>KI/KI</sup> mice. **e** Serum anti-dsDNA

total Ig.  $n = 8$  Ctrl vs 6 hWDFY3<sup>KI/KI</sup> mice. **f** PAS staining of kidney sections for the quantification of glomerular size.  $n = 7$  Ctrl vs 6 hWDFY3<sup>KI/KI</sup> mice. Scale bar = 25 μm. **g, h** Immunofluorescence staining of kidney sections using anti-C1q and anti-IgG antibodies (red) and WGA (green) to outline glomeruli. Mean fluorescent intensity (MFI) of C1q (**g**) and IgG (**h**) in the glomeruli area were quantified.  $n = 7$  Ctrl vs 6 hWDFY3<sup>KI/KI</sup> mice. NC negative control. Scale bar = 100 μm. Data are shown as mean ± SEM. A two-tailed Student's *t*-test was applied to all data.

schematic design). Middle-aged hWDFY3<sup>KI/KI</sup> mice showed enhanced macrophage efferocytosis (Supplementary Fig. 10b), lower kidney and lymph node (LN) weight (Supplementary Fig. 10c), lower ALT levels (Supplementary Fig. 10d), and reduced ANA total Ig and anti-dsDNA total Ig (Supplementary Fig. 10f, g), compared to middle-aged Ctrl mice, while creatinine level remained low and comparable (Supplementary Fig. 10e). Additionally, middle-aged hWDFY3<sup>KI/KI</sup> mice exhibited smaller glomeruli (Supplementary Fig. 10h) and lower IgG deposition in the kidney (Supplementary Fig. 10i) compared to age-matched Ctrl mice.

Collectively, these findings highlight the potential therapeutic opportunity of WDFY3 overexpression to mitigate autoimmunity driven by increased dead cell burden and age-associated chronic inflammation.

### Overexpression of WDFY3 in macrophages mitigates T cell activation and IL-1β secretion in response to the efferocytosis of ACs

We next examined whether WDFY3 overexpression suppresses T cell activation and cytokine dysregulation (Fig. 6). The percentage of CD44<sup>hi</sup>CD62L<sup>lo</sup> activated T cells in CD4<sup>+</sup> and CD8<sup>+</sup> T cells, as well as CXCR3<sup>+</sup> activated T cells in CD4<sup>+</sup> and CD8<sup>+</sup> T cells in the blood, showed a modest reduction in hWDFY3<sup>KI/KI</sup> mice (Fig. 6b, c). The percentage of CD44<sup>hi</sup>CD62L<sup>lo</sup> activated T cells in splenic CD4<sup>+</sup> and CD8<sup>+</sup> T cells also decreased in hWDFY3<sup>KI/KI</sup> mice (Fig. 6d). hWDFY3<sup>KI/KI</sup> mice showed decreased MHC-II-mediated antigen presentation to CD4<sup>+</sup> T cells in vivo (Fig. 6e). We also observed lower serum IL-18 levels in 15-month-

old hWDFY3<sup>KI/KI</sup> mice compared to Ctrl (Fig. 6f). The hWDFY3<sup>KI/KI</sup> mice showed decreased pro-IL-1β expression and caspase-1 cleavage in F4/80<sup>+</sup> splenic macrophages (Fig. 6g, h). Additionally, AC-induced IL-1β secretion was lower in hWDFY3<sup>KI/KI</sup> BMDMs (Fig. 6i). To assess the effects of WDFY3 overexpression on efferocyte-T cell interaction, BMDMs were co-incubated with ACs to induce efferocytosis, followed by co-culture with CFSE-labeled CD4<sup>+</sup> T cells to assess T cell expansion and activation. hWDFY3<sup>KI/KI</sup> efferocyte suppressed T cell expansion and effector T cell differentiation, while promoting Treg differentiation (Fig. 6j, Supplementary Fig. 7b for gating strategies). Taken together, WDFY3 overexpression suppresses MHC-II-mediated antigen presentation and IL-1β secretion by efferocytes, thereby attenuating efferocyte-T cell interaction and T cell activation. Notably, WDFY3 overexpression had a minimal impact on steady-state gene expression; RNA-seq analysis of BMDMs from Ctrl and hWDFY3<sup>KI/KI</sup> mice identified only 13 differentially expressed genes, none of which are directly involved in regulating antigen presentation or IL-1β secretion (Supplementary Data 2), suggesting that WDFY3 likely exerts its effects through non-transcriptional mechanisms.

### Discussion

Our work advances several conceptual ideas on macrophage efferocytosis in autoimmunity. First, we identified a significant role for the myeloid-specific knockout of *Wdfy3* in promoting autoimmune responses, both in young mice with an increased AC burden and in middle-aged mice developing spontaneous autoreactivity. This phenotype involves impaired efferocytosis, leading to autoantigen-



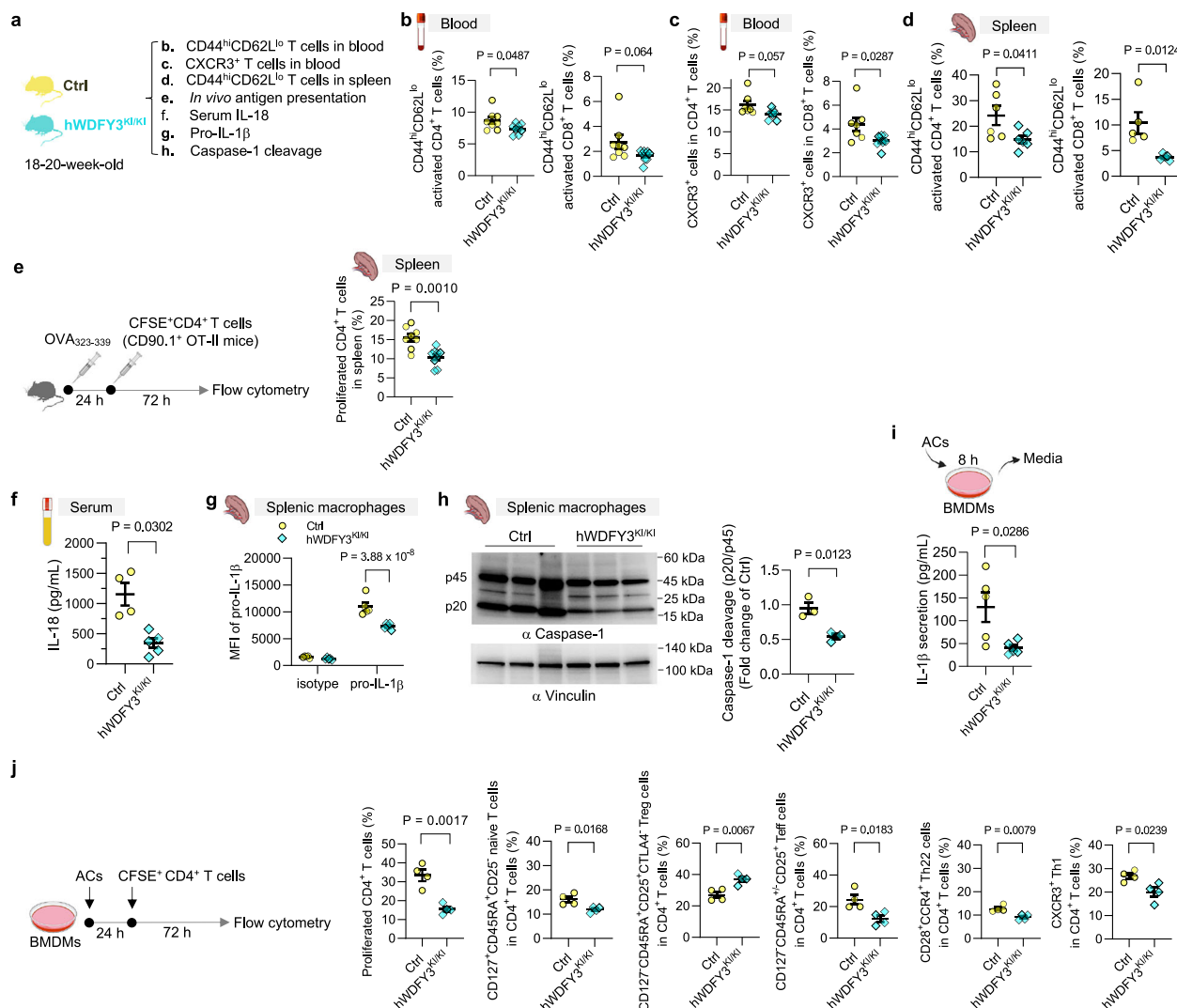


**Fig. 6 | Overexpression of *WDFY3* suppresses T cell activation by restraining macrophage antigen presentation and inflammasome activation.** **a** Schematic of study design. Ctrl and hWDFY3<sup>KI/KI</sup> littermates were used to assess T cell activation (b–d), antigen presentation (e), inflammasome activation (f–i), and (j) efferocyte-T cell interaction. **b** The percentage of CD44<sup>high</sup>CD62L<sup>low</sup> activated T cells in CD4<sup>+</sup> and CD8<sup>+</sup> T cells in the blood.  $n = 8$  Ctrl vs 8 hWDFY3<sup>KI/KI</sup> mice for CD4<sup>+</sup> T cells;  $n = 8$  Ctrl vs 9 hWDFY3<sup>KI/KI</sup> mice for CD8<sup>+</sup> T cells. **c** The percentage of CXCR3<sup>+</sup> activated T cells in CD4<sup>+</sup> and CD8<sup>+</sup> T cells in the blood.  $n = 8$  Ctrl vs 9 hWDFY3<sup>KI/KI</sup> for CD4<sup>+</sup> T cells;  $n = 7$  Ctrl vs 8 hWDFY3<sup>KI/KI</sup> mice for CD8<sup>+</sup> T cells. **d** The percentage of CD44<sup>high</sup>CD62L<sup>low</sup> activated T cells in splenic CD4<sup>+</sup> and CD8<sup>+</sup> T cells.  $n = 6$  Ctrl vs 6 hWDFY3<sup>KI/KI</sup> mice for CD4<sup>+</sup> T cells;  $n = 5$  Ctrl vs 5 hWDFY3<sup>KI/KI</sup> mice for CD8<sup>+</sup> T cells. **e** In vivo antigen presentation assay. Mice were immunized with OVA<sub>323-339</sub> for 24 h before the injection of CFSE-labeled splenic CD4<sup>+</sup> T cells from CD90.1<sup>+</sup> OT-II mice. Seventy-two hours after injection, CFSE dilution in CD4<sup>+</sup>CD90.1<sup>+</sup> splenic T cells was assessed.  $n = 8$  Ctrl vs 9 hWDFY3<sup>KI/KI</sup> mice. **f** Serum IL-18 in 15-month-old mice.  $n = 4$

Ctrl vs 5 hWDFY3<sup>KI/KI</sup> mice. **g** The expression of pro-IL-1 $\beta$  in F4/80<sup>+</sup> splenic macrophages assessed by flow cytometry. MFI, median fluorescence intensity.  $n = 5$  Ctrl vs 5 hWDFY3<sup>KI/KI</sup> mice. **h** Analysis of intracellular caspase-1 cleavage in F4/80<sup>+</sup> splenic macrophages by Western blotting. The ratio of p20 intensity to p45 intensity was calculated, and this ratio was normalized to the control group (Ctrl), which was assigned a value of 1.0 for standardization.  $n = 3$  Ctrl vs 3 hWDFY3<sup>KI/KI</sup> mice. **i** BMDMs were co-incubated with ACs at a 5:1 AC-to-BMDM ratio for 8 h. Culture media were collected to determine IL-1 $\beta$  by ELISA.  $n = 5$  Ctrl vs 5 hWDFY3<sup>KI/KI</sup> mice. **j** Efferocyte-T cell interaction. BMDMs were co-incubated with ACs for 24 h and then removed by washing, followed by co-culture with CFSE-labeled CD4<sup>+</sup> splenic T cells for 72 h to assess efferocyte-mediated activation of CD4<sup>+</sup> T cells.  $n = 4$  Ctrl vs 4 hWDFY3<sup>KI/KI</sup> mice. Data are shown as mean  $\pm$  SEM. A two-tailed Student's *t*-test was applied to all data, except for (g), where a two-way ANOVA was performed, followed by Sidak's post hoc test to adjust for multiple comparisons.

triggered autoantibody formation and immune complex deposition, most notably in the kidney. Mechanistically, macrophages, as the efferocytes, can activate CD4<sup>+</sup> T cells upon engulfing ACs, suggesting that the process of efferocytosis directly impacts macrophage function in ways that amplify autoimmune responses. WDFY3 plays a critical role in regulating macrophage-T cell interaction by suppressing MHC-II-mediated antigen presentation and cytokine dysregulation, beyond its role in limiting autoantigen release. Finally, WDFY3 overexpression enhances macrophage efferocytosis, reduces AC-induced IL-1 $\beta$  secretion, suppresses T cell

activation, and protects mice from both AC-induced and age-associated autoimmune phenotypes.

It is worth noting that efferocytosis, particularly following the degradation of the AC corpses, induces the production of anti-inflammatory cytokines such as transforming growth factor-beta (TGF- $\beta$ ) and interleukin-10 (IL-10), thereby promoting the resolution of inflammation<sup>38–41</sup>. Our work reveals that macrophage responses to AC engulfment involve modest IL-1 $\beta$  secretion and CD4<sup>+</sup> T cell activation, both of which are exacerbated by *Wdfy3* knockout and suppressed by WDFY3 overexpression. The molecular mechanisms underlying these

effects remain to be defined. Given that WDFY3 overexpression or knockout in BMDMs induces only minimal transcriptomic changes<sup>19</sup>, we speculate that WDFY3 primarily functions through protein-protein interactions. Additionally, WDFY3 localizes to RAB5- and EEA1-positive early endosomes<sup>42</sup>, where it may regulate antigen processing and peptide loading to MHC-II<sup>43,44</sup>. In neuronal cells, WDFY3 acts as an adaptor protein in autophagy-mediated degradation of protein aggregate<sup>45–48</sup>, suggesting a potential parallel mechanism in macrophages. Whether WDFY3 scaffolds or targets specific protein complexes for degradation in this context warrants further investigation. Nevertheless, our study uncovers macrophage WDFY3 as a key regulator that enhances efferocytosis while suppressing antigen presentation and cytokine dysregulation, thereby amplifying the inflammation-resolving benefits of efferocytosis. These findings also support a broader view of efferocytosis as an active immunomodulatory process and highlight WDFY3 as a potential target for reprogramming macrophage responses following efferocytosis.

Among immune cells, WDFY3 is abundantly expressed in monocytes and macrophages, with low expression in granulocytes, B cells and DCs<sup>19</sup>. Beyond immune cells, WDFY3 is most abundantly expressed in neuronal cells, where it regulates the clearance of aggregated proteins through aggregophagy<sup>46,48</sup>. Ectopic overexpression of WDFY3 exerts neuroprotective effects in mice<sup>34</sup>. Although our work using constitutive whole-body overexpression mice does not exclude potential protective effects from other cell types, the essential role of macrophage WDFY3 as a protector against autoimmunity is well established using in vitro cultured murine and human macrophages and in vivo mouse models with myeloid-specific knockout. Our findings highlight the potential therapeutic applications of enhancing WDFY3 to mitigate autoimmune disorders associated with defective efferocytosis, as well as age-associated chronic inflammation<sup>49</sup>. Furthermore, our research opens avenues for exploring the protective role of macrophage WDFY3 in autoimmune disease models and across distinct tissue environment, in light of recent evidence that efferocytic clearance of different AC types elicits unique macrophage responses<sup>50,51</sup>.

## Methods

### Mice

Animal protocols were approved by the Institutional Animal Care and Use Committee at Columbia University (Protocol Number AC-AABN5558). Mice were housed socially in standard cages at 22 °C with 40–60% humidity under a 12–12 h light-dark cycle within specific pathogen-free (SPF) facilities. Experimental and control mice were co-housed in the same cage whenever possible to minimize environmental variation. *Ad libitum* access to water and food is provided by the facility (PicoLab Rodent Diet 20 5053 and 5058, LabDiet). Myeloid-specific *Wdfy3* knockout mice were generated by crossing *Wdfy3*<sup>fl/fl</sup> (generated Dr. Ai Yamamoto's lab<sup>20</sup> and backcrossed to C57BL/6 J mice for nine generations) with *LysMCre*<sup>+/−</sup> (Stock No. 004781, the Jackson Laboratory)<sup>21</sup>. *LysMCre*<sup>+/−</sup>*Wdfy3*<sup>fl/fl</sup> mice (Cre<sup>+</sup>) had myeloid-specific knockout of *Wdfy3*, while *LysMCre*<sup>+/−</sup>*Wdfy3*<sup>fl/fl</sup> littermates (Cre<sup>−</sup>) served as controls<sup>19</sup>. Mice overexpressing human *WDFY3* were generated by Dr. Ai Yamamoto's lab<sup>34</sup>. Specifically, the construct (the cDNA sequence encoding 3× FLAG tag that is fused to human *WDFY3* cDNA preceded by a STOP cassette flanked by *loxP* sites) was knocked into the *Rosa26* locus (*Rosa26*<sup>loxP-STOP-loxP-3xFLAG-hWDFY3/+</sup>) and the expression driven by the endogenous *Rosa26* promoter. To achieve constitutive overexpression, male mice carrying the floxed allele were crossed with female carriers of *HprtCre*, a Cre-deleter strain with 100% Cre-mediated recombination in oocytes (Stock No. 004302, the Jackson Laboratory) to generate heritable deletion of *loxP-STOP-loxP* cassette (*Rosa26*<sup>3xFLAG-hWDFY3/+</sup>). *Rosa26*<sup>3xFLAG-hWDFY3/+</sup> mice were interbred to generate homozygotes, *Rosa26*<sup>3xFLAG-hWDFY3/3xFLAG-hWDFY3</sup>, for knock-in (KI) of 3xFLAG-hWDFY3 (hWDFY3<sup>KI/KI</sup>) and wildtype littermate controls (Ctrl). The hWDFY3<sup>KI/KI</sup> mice are on a mixed background (~81% C57BL/6 and ~19%

129/SvEv). The OT-I mice (Stock No. 003831)<sup>52</sup>, OT-II mice (Stock No. 004149)<sup>53</sup>, and CD90.1 (Thy 1.1) mice (Stock No. 000406) were obtained from the Jackson Laboratory and used at 6–20 weeks of age. The genotype and age of mice used in each experiment are indicated in the corresponding figures and figure legends. Both sexes were included, with age- and sex matched pairs used for each genotype in all experiments. As our previous study showed that myeloid-specific *Wdfy3* knockout impairs efferocytosis in both males and females<sup>19</sup>, data were not further disaggregated by sex in this study.

Inclusion and exclusion criteria were established for the mouse cohorts in this study. Inclusion criteria required age- and sex-matched littermates that could be genotyped. Exclusion criteria included mice that died prematurely due to causes unrelated to experimental conditions (e.g., congenital defects or fighting). No differences in mortality rates were observed across groups up to middle-aged time points (approximately 52–60 weeks, or 12–14 months of age). Attrition due to technical or equipment errors during sample collection and processing after euthanasia was also accounted for, with affected samples excluded to ensure data reliability.

### Murine bone marrow-derived macrophages

Murine bone marrow-derived macrophages (BMDM) were prepared by differentiating bone marrow (BM) cells isolated from femurs and tibia<sup>19</sup>. BM cells were plated in 6-well non-tissue-culture (TC)-treated plates at  $2 \times 10^6$  to  $3 \times 10^6$  cells per well in DMEM basal medium (Fisher Scientific, 11-995-073) supplemented with 10% heat-inactivated (HI)-FBS (Gibco, A5256801), 20% L-929 cell-conditioned medium, and 2 mM L-Glutamine (Fisher Scientific, 25-030-081)<sup>19</sup>. BM cells were fully differentiated into BMDMs by day 7 for in vitro assay<sup>19</sup>.

### Murine peritoneal macrophages

Mouse peritoneal macrophages (PM) were prepared by collecting peritoneal exudates. The exudates were centrifuged at  $400 \times g$  for 5 min to obtain cell pellets, which were resuspended and plated in 12-well non-TC-treated plates at  $0.5 \times 10^6$  cells per well in DMEM basal medium supplemented with 10% HI-FBS, 20% L-929 cell-conditioned medium, and 2 mM L-Glutamine<sup>19</sup>. Unattached cells were removed 6–8 h after plating, and the attached cells were cultured for an additional 12–18 h to allow full spreading before performing efferocytosis assay<sup>19</sup>.

### Murine splenic macrophages

Spleen single-cell suspensions were prepared by pressing spleens through 70  $\mu$ m cell strainers (Fisher Scientific, 22-363-548)<sup>54</sup>. F4/80<sup>+</sup> splenic macrophages were captured and purified by positive selection using magnetic separation of F4/80<sup>+</sup> cells (Fisher Scientific, 50-112-5082), following the manufacturer's protocol.

### Human monocyte-derived macrophages

Human monocyte-derived macrophages (HMDM) were differentiated from peripheral blood mononuclear cells (PBMC)<sup>19</sup>. PBMCs were isolated from buffy coats of anonymous, de-identified healthy adult volunteer donors (purchased from the New York Blood Center) by Ficoll (Fisher Scientific, 45-001-751) density gradient centrifugation<sup>19</sup>, and were either used fresh or cryopreserved. PBMCs were cultured in RPMI-1640 basal medium (Fisher Scientific, MT10040CM) supplemented with 20% HI-FBS and 50 ng/mL human macrophage colony-stimulating factor (M-CSF) (Thermo Fisher Scientific, 300-25-50UG) for 7–8 days<sup>19,55</sup>.

### Murine bone-marrow derived dendritic cells

BMs were plated in 6-well non-tissue-culture (TC)-treated plates at  $2 \times 10^6$  to  $3 \times 10^6$  cells per well in DMEM basal medium supplemented with 10% HI-FBS, 20 ng/mL GM-CSF (Peprotech, 315-03-50) and 20 ng/mL IL-4 (Peprotech, 214-14-50)<sup>25</sup>. Fresh media were added every 2 days. On day 6, the cell suspension was collected by gently agitating and

pipetting the culture. The cell suspension was then centrifuged, and the resulting cell pellet was resuspended in fresh media and returned to the original plate. On day 8, BM-derived dendritic cells (BMDC) were ready for experiments<sup>25</sup>. The percentage of CD11c<sup>+</sup> BMDCs was determined by flow cytometry (BioLegend, 117333, 1:50).

### Preparation of apoptotic cells and fluorescent labeling for efferocytosis assays

Apoptotic cells (AC) were generated by exposing isolated mouse thymocytes to ultraviolet light (UV, 254-nm wavelength) irradiation using a UVP EL Series UV Lamp (Analytik Jena US, Upland, CA; Model UVS-18, 95-0200-01) as described<sup>19,56,57</sup>. Briefly, single-cell suspension of mouse thymi of C57BL/6J wild-type mice were isolated and seeded in 10-cm non-TC-treated dish at  $1 \times 10^7$  cells per mL in 8 mL  $1 \times$  Dulbecco's Phosphate-Buffered Salt Solution without calcium and magnesium (DPBS, Fisher Scientific, MT21031CM), and then irradiated for a total of 15 min. Cell suspensions were then incubated at 37 °C with 5% CO<sub>2</sub> for 2.5 h. Annexin V staining (Invitrogen, A23204) was performed to confirm >90% apoptosis induction.

Fluorescent labeling of ACs was performed as described<sup>19</sup>. For single staining, ACs were labeled with 2  $\mu$ M Hoechst 33342 (Thermo Fisher Scientific, 62249) for 30 min or 10  $\mu$ g/mL TAMRA (Thermo Fisher Scientific, C1171) for 25 min. For co-labeling with Hoechst 33342 and pHrodo-Red (Thermo Fisher Scientific, P36600), ACs were first stained by 2  $\mu$ M Hoechst 33342 for 30 min, followed by staining with 20 ng/mL pHrodo-Red for 25 min<sup>58</sup>. After washing the ACs with a 10-fold volume of PBS (Corning, 21-040-CV), ACs were used for efferocytosis assays.

### In vitro efferocytosis assay

As we described<sup>19,58</sup>, macrophages were differentiated in 6-well non-TC-treated plates to reach a density of  $\sim 1 \times 10^6$  differentiated macrophages per well. Fluorescently labeled ACs were co-incubated with macrophages at a 5:1 AC-to-macrophage ratio for 1 h in 2 mL DMEM basal medium supplemented with 10% HI-FBS at 37 °C, 5% CO<sub>2</sub>. Macrophages were then washed with  $1 \times$  DPBS gently for 5 times to remove unbound ACs. For flow cytometry-based quantification, macrophages were lifted using CellStripper (Corning, 25-056-CI), a non-enzymatic cell dissociation solution, for live-cell analysis.

### In vivo thymus efferocytosis assay

Mice were injected intraperitoneally with 200  $\mu$ L PBS containing 250  $\mu$ g dexamethasone (Sigma-Aldrich, 265005-100MG) as previously described<sup>19</sup>. 18 h after injection, mice were euthanized, and thymi were dissected and weighed. One lobe was immersed in optimal cutting temperature (OCT) compound (Fisher Scientific, 23-730-571) and snap-frozen for immunofluorescence staining to determine efferocytosis in situ<sup>19</sup>. Frozen sections were stained with terminal deoxynucleotidyl transferase dUTP nick end labeling (TUNEL, Thermo Fisher Scientific, C10618) to label ACs and CD68 antibody (Abcam, ab53444, 1:50) to label macrophages. The ratio of macrophage-associated ACs to free ACs was calculated to represent the capability of efferocytosis by thymus macrophages<sup>19</sup>. The other lobe was disaggregated into single cells to count the total number of cells and quantify the percentage of Annexin V<sup>+</sup> ACs using Annexin V Cellular Apoptotic kit (Invitrogen, A23204) by flow cytometry.

### In vivo peritoneal macrophage efferocytosis assay

Mice were injected intraperitoneally with  $1 \times 10^7$  TAMRA-stained apoptotic mouse thymocytes in 300  $\mu$ L PBS. Fifteen minutes after injection, mice were euthanized, and peritoneal exudates were collected. The pelleted cells were blocked with CD16/32 (BioLegend, 101302, 1:200) and then stained with F4/80-APC antibody (BioLegend, 123116, 1:100) for 15 min on ice to label macrophages. The percentage of TAMRA<sup>+</sup> PMs was determined by flow cytometry<sup>19</sup>.

### Induction of autoimmune-like responses via repeated AC injections

Exposure to large numbers of ACs was used to evoke immune responses in mice as previously described<sup>22</sup>. Thymocytes from C57BL/6J wild-type mice were UV-irradiated to induce apoptosis and  $2 \times 10^7$  ACs per mouse were injected intravenously via tail vein injection. The injections were performed weekly for 4 weeks, paused for 2 weeks, followed by 2 additional injections at week 7 and week 8. One week after the last injection, mice were euthanized to collect serum and kidneys to assess immune responses.

### Single AC injection to assess accumulation in different organs

To determine AC accumulation in different organs upon injection, ACs were labeled with 10  $\mu$ g/mL TAMRA (Thermo Fisher Scientific, C1171) for 25 min and  $2 \times 10^7$  ACs per mouse were injected intravenously via tail vein injection<sup>59</sup>. 24 h or 48 h post injection, mice were euthanized to harvest spleen, liver, and kidney. Control groups were injected with sterile PBS and were euthanized 48 h post-injection. Single cell suspensions of spleen<sup>54</sup>, liver<sup>60</sup>, and kidney (Miltenyi Biotec, 130-110-203) were prepared to determine the percentage of TAMRA<sup>+</sup> cells by flow cytometry. Cell suspensions from the control groups were used to assess autofluorescence and to guide gating strategies.

### Assessment of autoimmunity-related phenotypes in mice

Organ weight: Spleen, kidney, and subiliac lymph node (LN) were dissected and weighed.

Serum alanine aminotransferase and creatinine: Peripheral blood was collected to obtain serum by centrifuging at  $1400 \times g$  for 10 min at 4 °C. Serum alanine aminotransferase (ALT) and creatinine were determined using a Heska Element DCSX Veterinary Chemistry Analyzer with 120  $\mu$ L serum delivered on ice and analyzed by the diagnostic lab at the Institute of Comparative Medicine (ICM), Columbia University Irving Medical Center.

Serum autoantibodies: Serum antinuclear antibodies (ANA) and anti-dsDNA antibodies were determined using mouse antinuclear antigens Ig's (Total A + G + M) ELISA kit (Alpha Diagnostics International, 5210), mouse anti-nuclear antibody (IgG) ELISA Kit (CUSABIO, CSB-E12912m) and mouse anti-dsDNA Ig's (Total A + G + M) ELISA kit (Alpha Diagnostics International, 5110).

Histopathological analysis of mouse kidney, spleen, liver and skin: Kidney, spleen, liver, and skin were harvested at euthanasia and immersion-fixed in 4% formaldehyde (Thermo Fisher Scientific, 28908), embedded in paraffin, and coronal sections cut at 3  $\mu$ m thickness<sup>25</sup>. Hematoxylin and eosin (H&E) staining was performed to grade for potential pathologic features of systemic lupus erythematosus (SLE) organ involvement on a semiquantitative scale of 0, 1+, 2+, 3+, as listed in Supplementary Data 1. For the degree of mesangial hypercellularity, 0 = none; 1+ = mild; 2+ = moderate; 3+ = severe hypercellularity. For the degree of endocapillary hypercellularity/leukocyte infiltration, 1+ = involving <25% glomeruli; 2+ = involving 25–50% glomeruli; 3+ = involving >50% glomeruli. Grading was performed blindly by a pathologist (V.D.D.).

Glomerular area and immune complex deposition in the glomeruli: kidneys were embedded in optimal cutting temperature (OCT) compound and snap frozen. Cryostat sections were cut at 3  $\mu$ m for periodic acid-Schiff (PAS) staining (Sigma-Aldrich, 395B) and for indirect immunofluorescent staining. For PAS staining, frozen sections were fixed with 4% formaldehyde for 20 min at room temperature. Cross sections were imaged with the Leica Aperio AT2 Slide Scanner. Glomeruli along the longitudinal line and the transverse line of the cross section were identified. Glomerular area was quantified and presented as the mean area of 12–15 glomeruli per mouse using the Aperio ImageScope software (Leica, V12.4.6.5003)<sup>25</sup>. For immunofluorescence staining of C1q, IgG, or wheat germ agglutinin (WGA)<sup>61,62</sup>, frozen sections were fixed with 4%



formaldehyde for 20 min at room temperature. Permeabilization using 0.5% Triton X-100 in PBS was followed by blocking with 5% BSA in PBS-0.05% Tween-20 (PBST). Slides were washed with PBST for three to five times between each step. For CIq staining, primary antibody incubation was carried out overnight at 4 °C using rabbit monoclonal to CIq (Abcam, ab182451, 1:50), followed by secondary antibody incubation for 1 h at room temperature using Alexa-Fluor 555-goat anti rabbit IgG (H + L) (Invitrogen, A21428, 1:200). For IgG or WGA staining, Alexa-Fluor 555-conjugated anti-IgG (Invitrogen, A21422, 1:200) or Alexa-Fluor 488-conjugated WGA (Invitrogen, W11261, 1:5000) were used. DAPI (Invitrogen, P36931, 1:5000) was used to stain nuclei. Negative controls were included using rabbit IgG isotype control (Cell Signaling Technology, 3900S, 1:50). Slides were mounted with antifade mountant (Invitrogen, P36930) and imaged using the ImageXpress Micro4 high-content microscopy with a Nikon Plan Apo  $\lambda$  20 $\times$ /0.75 objective (Molecular Device) or Nikon Ti-S Automated Inverted Microscope (Nikon). The mean fluorescence intensity (MFI) within the glomeruli area was quantified by analyzing 20–25 glomeruli from two sections per mouse using Image J 1.53 u.

### Characterization of splenic and liver macrophages by flow cytometry and immunofluorescence staining

Single-cell suspensions of spleen<sup>54</sup> and liver<sup>60</sup> were prepared and stained with antibodies against CD45-PE-Cy7 (BioLegend, 109830, 1:100), CD11b-PB (BioLegend, 101224, 1:100), Ly6C-APC (BioLegend, 128015, 1:100), Ly6G-PE (BioLegend, 128015, 1:100), and F4/80-FITC (BioLegend, 123108, 1:100)<sup>50</sup>. To determine the expression of efferocytic receptors in splenic or liver macrophages, cell suspensions were stained with antibodies against CD45-APC-Cy7 (BD Biosciences, 557659, 1:100), CD11b-PB (BioLegend, 101224, 1:100), F4/80-FITC (BioLegend, 123108, 1:100), MerTK-PE (BioLegend, 151505, 1:100), AXL-PE-Cy7 (Invitrogen, 25-1084-82, 1:100), and TIM4-APC (Invitrogen, 46-5866-82, 1:100)<sup>50</sup>. A NovoCyte flow cytometer (Agilent Technologies) was used to determine the percentage of macrophages and surface efferocytic receptor expression.

For immunofluorescence staining of CD68, paraffin sections were used<sup>63</sup>. After deparaffinization and rehydration, antigen retrieval was performed using a steamer in antigen unmasking solution (Vector, H-3300) for 18 min, followed by permeabilization and staining using CD68 antibody (Abcam, ab53444, 1:50) and secondary antibody Alexa-Fluor 555-goat anti rat IgG (H + L) (Invitrogen, A21434, 1:200). DAPI (Invitrogen, P36931, 1:5000) was used to stain nuclei. Slides were mounted with antifade mountant (Invitrogen, P36930) and imaged using a Nikon Ti-S Automated Inverted Microscope (Nikon). The macrophage zone in the spleen and macrophage count in the liver were quantified by analyzing two sections per mouse using Image J 1.53 u.

### Western blotting

Cells from one-well of 6-well plate, i.e., about  $1 \times 10^6$  cells, were harvested using Cell Stripper (Corning, 25-056-CI). The cell pellet was then lysed on ice for 30 min in 70  $\mu$ L 1 $\times$  RIPA buffer (MilliporeSigma, 20-188) supplemented with protease inhibitor cocktail and phosphatase inhibitor cocktail<sup>64</sup>, followed by centrifugation at 12,000  $\times g$  for 10 min at 4 °C. Protein lysates were similarly prepared from F4/80<sup>+</sup> splenic macrophages, which were isolated by positive selection using magnetic separation (Fisher Scientific, 50-112-5082). The supernatants were transferred to fresh tubes and mixed with 5 $\times$  SDS sample buffer (250 mM Tris-HCl, pH 6.8, 20% SDS, 30% (v/v) Glycerol, 10 mM DL-Dithiothreitol (DTT), 0.05% (w/v) Bromophenol blue). Samples were loaded onto a 3–8% Tris-Acetate gel (Thermo Fisher Scientific, EA0378BOX) and then transferred to 0.45  $\mu$ m PVDF membrane (Thermo Fisher Scientific, 88518). Blocking was performed in 5% milk in TBST at room temperature for 1 h. Primary

antibody incubation was carried out at 4 °C overnight, followed by incubation with secondary antibodies at room temperature for 1 h. Primary antibodies used for this study include anti-WDFY3 (a gift from Ai Yamamoto lab, 1:1000)<sup>34</sup>, anti-caspase-1 (mouse, eBioscience, 14-9832, 1:1000), and anti-caspase-1 (human, Thermo Fisher Scientific, MA547253, 1:500). Secondary antibodies include HRP-conjugated goat-anti-rabbit IgG (Cell Signaling Technology, 7074, 1:5000) and HRP-conjugated goat-anti-rat IgG (Cell Signaling Technology, 7077, 1:5000). Housekeeping protein antibodies include HRP-conjugated rabbit-anti-GAPDH (Cell Signaling Technology, 3683S, 1:5000), HRP-conjugated rabbit-anti- $\beta$ -Actin (Cell Signaling Technology, 5125S, 1:2000), and HRP-conjugated rabbit-anti-Vinculin (Cell Signaling Technology, 18799S, 1:2000). Target protein and the respective housekeeping protein are derived from the same membrane.

### T cell activation by flow cytometry

T cell activation was characterized in blood T cells and splenic T cells in mice as previous described<sup>25</sup>. Blood samples were collected into a blood collection tubes with sodium heparin. Red blood cells (RBCs) were lysed by using ice-cold RBC lysis buffer (Invitrogen, 50-112-9751) for 10 min on ice. White blood cells were pelleted, washed, and resuspended in ice-cold washing buffer containing 2% HI-FBS, 5 mM EDTA (Thermo Fisher Scientific, 15-575-020), 1 mM sodium pyruvate (Fisher Scientific, 11-360-070), and 20 mM HEPES (Fisher Scientific, MT25060CI) in 1 $\times$  DPBS. Spleen single-cell suspensions were prepared by pressing spleens through 70  $\mu$ m strainers, followed by RBC lysis<sup>54</sup>. Cell suspensions were stained with an antibody cocktail against CD45-APC-Cy7 (BD Pharm, 557659, 1:100), Ly6-C/G-PerCP-Cy5.5 (BD Pharm, 552093, 1:100), CD115-PE (Invitrogen, 12-1152-83, 1:100), TCR $\beta$ -PB (BioLegend, 109226, 1:100), CD44-PE-Cy7 (Invitrogen, 25-0441-82, 1:100), CD62L-APC (Invitrogen, 17-0620-82, 1:100) or CXCR3-APC (Invitrogen, 17-1831-82, 1:100), CD8-FITC (eBioscience, 11-0083-85, 1:100) or CD4-FITC (BioLegend, 100406, 1:100). CD4<sup>+</sup> T cells were recognized as CD45<sup>+</sup>Ly6-C/G-CD115<sup>+</sup>TCR $\beta$ <sup>+</sup>CD4<sup>+</sup> or CD45<sup>+</sup>Ly6-C/G-CD115<sup>+</sup>TCR $\beta$ <sup>+</sup>CD8<sup>+</sup>. The CD8<sup>+</sup> T cells were recognized as CD45<sup>+</sup>Ly6-C/G-CD115<sup>+</sup>TCR $\beta$ <sup>+</sup>CD8<sup>+</sup>. The active form of CD4<sup>+</sup> and CD8<sup>+</sup> T cells were identified as CD44<sup>+</sup>CD62L<sup>+</sup> or CXCR3<sup>+</sup> using a NovoCyte flow cytometer.

### T cell subset characterization by flow cytometry

For CD4<sup>+</sup> T cell subset characterization<sup>65</sup>, cell suspensions were stained with antibodies against CD4-FITC (BioLegend, 100406, 1:100), CD25-PB (BioLegend, 102021, 1:100), CD45RA-PE (BD Pharmingen, 553380, 1:100), CD127-APC-Cy7 (BioLegend, 135039, 1:100), CTLA4-APC (BioLegend, 106309, 1:100). To characterize Th1 and Th22 CD4<sup>+</sup> T cells, cell suspensions were stained with antibodies against CD4-PB (Invitrogen, 48-0041-82, 1:100), CXCR3-FITC (BioLegend, 126535, 1:100), CCR4-PE (BioLegend, 131203, 1:100), and CD28-PE-Cy7 (BioLegend, 102125, 1:100). For CD8<sup>+</sup> T cell subset characterization<sup>65</sup>, cell suspensions were stained with antibodies against CD8a-FITC (Invitrogen, 11-0081-85, 1:100), CCR7-APC (BioLegend, 120107, 1:100), CD62L-APC-Cy7 (BioLegend, 104427, 1:100), and CD45RA-PE. To determine intracellular IFN- $\gamma$  in T cells, cells were fixed and permeabilized using BD Cytofix/Cytoperm Fixation/Permeabilization kit (BD Biosciences, 554714), stained with IFN- $\gamma$ -APC (BioLegend, 505810, 1:50) or its isotype control (BioLegend, 400411, 1:50). To determine MHC-II and MHC-I expression in BMDMs, BMDMs were harvested and stained by MHC-I-PE-Cy7 (BioLegend, 114717, 1:100), MHC-II-APC-Cy7 (BioLegend, 107627, 1:100), and F4/80-FITC (BioLegend, 123108, 1:100). For in vivo antigen presentation assay, CD90.1-FITC (BioLegend, 109008, 1:100) or CD90.1-PB (BioLegend, 202522, 1:100) were used to identify the donor T cells. A NovoCyte flow cytometer was used to analyze the percentage of T cell populations and the expression of intracellular or cell surface markers.

### In vitro antigen presentation assay

MHC-II and MHC-I mediated antigen presentation by BMDMs in vitro was assessed using ovalbumin (OVA) peptides and OT-II and OT-I transgenic T cells, as modified from previously published protocols<sup>25,26,66</sup>. CD4<sup>+</sup> T cells or CD8<sup>+</sup> T cells were isolated from spleen single-cell suspensions of OT-II mice or OT-I mice, respectively, using CD4 (Miltenyi Biotec, 130-117-043) or CD8a (Miltenyi Biotec, 130-117-044) MicroBeads. Isolated T cells were labeled with 5  $\mu$ M carboxy-fluorescein succinimidyl ester (CFSE)-Violet Proliferation Dye 450 (VPD450, BD Horizon, 562158) for 25 min. For MHC-II-mediated antigen presentation, BMDMs were pulsed with OVA<sub>323-339</sub> peptide (20  $\mu$ g/mL, Anaspec, 50-843-886) for 24 h, followed by co-culture with CD4<sup>+</sup> OT-II T cells for 72 h. For MHC-I-mediated antigen presentation, BMDMs were pulsed with OVA<sub>257-264</sub> peptide (20  $\mu$ g/mL, Anaspec, 50-844-730) for 24 h, followed by co-culture with CD8<sup>+</sup> OT-I T cells for 72 h. T cell proliferation was assessed by measuring CFSE-VPD450 dilution in CD4<sup>+</sup> T cells (CD4-APC, Invitrogen, 17-0041-81, 1:100) or CD8<sup>+</sup> T cells (CD8a-FITC, Invitrogen, 11-0081-82, 1:100) using a NovoCyte flow cytometer, as each round of division corresponds to a reduction in CFSE-VPD450 fluorescence intensity, thereby serving as a marker for T cell proliferation.

### In vivo antigen presentation assay

To assess antigen presentation in vivo, mice were immunized by subcutaneous injection of 100  $\mu$ L per mouse of a 1:1 mixture of immunogen (20  $\mu$ g OVA peptide in PBS) and Freund's Adjuvant (Sigma-Aldrich, F5881)<sup>25,67</sup>. 24 h after injection, mice received  $2 \times 10^6$  CD4<sup>+</sup>CD90.1<sup>+</sup> OT-II T-cells labeled with 10  $\mu$ M CFSE-VPD450. After 72 h, spleen single-cell suspensions were stained with CD4-APC (Invitrogen, 17-0041-81, 1:100) or CD8a-FITC (Invitrogen, 11-0081-85, 1:100) and CD90.1-PE (Invitrogen, 12-0900-83, 1:100) antibodies and analyzed using a NovoCyte flow cytometer. CD4<sup>+</sup>CD90.1<sup>+</sup> T cells with diluted CFSE-VPD450 indicated proliferation of CD4<sup>+</sup> T cells derived from CD90.1<sup>+</sup> OT-II donor mice. CD8<sup>+</sup>CD90.1<sup>+</sup> T cells with diluted CFSE-VPD450 indicated proliferation of CD8<sup>+</sup> T cells derived from CD90.1<sup>+</sup> OT-I donor mice.

### Assessment of efferocyte-T cell interaction

The method to assess efferocyte-T cell interaction to induce T cell activation was modified from a previously published protocol<sup>32</sup>. After UV irradiation to induce apoptosis, ACs were collected and centrifuged at  $500 \times g$ . The pelleted ACs were resuspended in  $1 \times$  DPBS supplemented with 2% HI-FBS and 2 mM EDTA at  $2 \times 10^7$ /mL, and incubated at 37 °C, 5% CO<sub>2</sub> overnight in sterile tubes. After overnight incubation, 0.5 mL cell suspensions were added to BMDMs in one well of 6-well plate and co-incubated for 24 h. After 24 h co-incubation, AC cell suspensions were removed by washing. CD4<sup>+</sup> T cells were isolated from spleen single-cell suspensions of mice using CD4 MicroBeads (Miltenyi Biotec, 130-117-043), followed by CFSE-VPD450 labeling, and then added to BMDMs for 72 h co-incubation. The dilution of CFSE was evaluated using a NovoCyte flow cytometer<sup>26,68</sup>.

### LC3 lipidation measurement by flow cytometry

BMDMs were incubated with TAMRA-labeled ACs at a 5:1 AC-to-BMDM ratio at 37 °C, 5% CO<sub>2</sub> for 1 h efferocytosis. Unbound ACs were washed away. BMDMs were collected and resuspended in 300  $\mu$ L cold  $1 \times$  DPBS with 20  $\mu$ g/mL digitonin and incubated on ice for 10 min to permeabilize cells and allow non-membrane-bound LC3 to be removed from cells. Permeabilized BMDMs were then centrifuged for 5 min at  $750 \times g$ , followed by incubation with Alexa Fluor 488-conjugated anti-LC3A/B antibody (Cell Signaling Technology, 13082S, 1:50) or isotype control (Cell Signaling Technology, 4340, 1:50) diluted in cold washing buffer ( $1 \times$  DPBS, 2% HI-FBS, 5 mM EDTA, 1 mM sodium pyruvate, and 20 mM HEPES) for 15 min on ice to stain the membrane-bound lipidated LC3-II within the cells<sup>69</sup>. After staining, macrophages were washed with cold washing buffer. Cell pellets were resuspended in

washing buffer and analyzed by flow cytometry by gating the TAMRA<sup>+</sup> BMDMs to quantify the median fluorescence intensity (MFI) of LC3A/B.

### Intracellular staining to determine Pro-IL-1 $\beta$ expression by flow cytometry

For the detection of pro-IL-1 $\beta$  in murine splenic macrophages, F4/80<sup>+</sup> cells were captured and purified from spleen single-cell suspensions by positive selection using magnetic separation (Fisher Scientific, 50-112-5082). F4/80<sup>+</sup> splenic macrophages were fixed and permeabilized using BD Cytofix/Cytoperm Fixation/Permeabilization kit (BD Biosciences, 554714), stained with pro-IL-1 $\beta$ -PE (eBioscience, 12-7114, 1:50) and its isotype control (eBioscience, 12-4301, 1:50), and analyzed by flow cytometry<sup>25</sup>.

### Immunofluorescence staining of ASC in BMDMs post-efferocytosis

BMDMs were co-incubated with TAMRA-labeled ACs for 15 min to initiate efferocytosis, after which unbound ACs were removed by washing. The BMDMs were then fixed with 4% formaldehyde for 30 min at room temperature. Permeabilization was performed using 0.5% Triton X-100 in PBS, followed by blocking with 5% BSA in PBST for 30 min. For ASC staining<sup>70</sup>, the cells were incubated overnight at 4 °C with a rabbit anti-ASC (AL177) polyclonal antibody (AdipoGen, AG-25B-0006-C100, 1:50), followed by 1 h incubation at room temperature with an AF488 goat anti-rabbit IgG (H + L) secondary antibody (Invitrogen, A11008, 1:200). Nuclei were counterstained with DAPI (Invitrogen, 62248, 1:10,000). Imaging was conducted using a Nikon Ti-S Automated Inverted Microscope equipped with a Plan Apo  $\lambda$  60 $\times$  oil objective. The mean fluorescence intensity (MFI) of ASC staining in efferocytes (BMDMs that engulfed ACs) was quantified using Image J 1.53 u.

### Cytokine and chemokine measurement in serum or culture media

The 26-plex ProcartaPlex Mouse Cytokine & Chemokine Convenience Panel 1 was used to analyze serum samples using Luminex xMAP technology (Thermo Fisher Scientific, EPXR260-26088-901)<sup>71</sup>. Serum IL-18 was determined using the mouse IL-18 DuoSet ELISA kit (R&D Systems, DY762505)<sup>25</sup>.

To determine how efferocytosis affect IL-1 $\beta$  secretion<sup>72</sup>, ACs were co-incubated with BMDMs for 8 h with a 5:1 AC-to-BMDM ratio, i.e.,  $5 \times 10^6$  ACs were added to one-well of 6-well plate of differentiated BMDMs, that generally contains  $\sim 1 \times 10^6$  BMDMs. Media were collected to determine secreted IL-1 $\beta$  using mouse IL-1 $\beta$ /IL-1F2 Quantikine ELISA kit (R&D Systems, MLB00C).

### siRNA-mediated gene silencing

Non-targeting siRNA control (si-Ctrl) (Dharmacon, D-001810-10-05) and WDFY3-targeting siRNA (si-WDFY3) (Dharmacon, L-012924-01-0005) were obtained from Dharmacon<sup>19</sup>. Human PBMCs were seeded at  $3 \times 10^6$  to  $5 \times 10^6$  per well of 6-well non-TC-treated plate for differentiation to HMDMs in RPMI-1640 basal medium supplemented with 20% HI-FBS and 50 ng/mL human M-CSF. On day 5, HMDMs were transfected with 25 pmol siRNAs using 7.5  $\mu$ L Lipofectamine RNAiMAX (Fisher Scientific, 13-778-075) in a total of 300  $\mu$ L Opti-MEM (Gibco, 31985070) for each well. On day 7, the culture media were refreshed before all treatments. To induce inflammasome activation<sup>73</sup>, HMDMs were primed by 20 ng/mL lipopolysaccharide (LPS) (Sigma-Aldrich, L3129) for 3 h followed by 1-h treatment of 2 mM ATP (Thermo Fisher Scientific, R0441). To determine how efferocytosis affect caspase-1 cleavage, ACs were co-incubated with HMDMs for 4 h with a 5:1 AC-to-HMDM ratio, i.e.,  $2.5 \times 10^6$  ACs were added to one-well of 6-well plate of differentiated HMDMs, that generally contained  $\sim 0.5 \times 10^6$  HMDMs. Unbound ACs were washed away and HMDMs were collected to determine caspase-1 cleavage by Western blotting.

### RNA-sequencing sample preparation and data analysis

BM cells were isolated from 6–8-week-old Ctrl and hWDFY3<sup>K<sup>fl</sup>/K<sup>fl</sup></sup> mice ( $n = 5$  male mice per genotype) and differentiated into BMDMs. Total RNAs were extracted from day 7 BMDMs using the Quick-RNA Mini-prep Plus kit (Zymo Research, R1057) and the assessment of RNA integrity was performed using an Agilent 2100 Bioanalyzer. With a minimum of 300 ng input RNA, strand-specific, poly(A) + libraries were prepared and sequenced at 20 million 100-bp paired-end reads per sample. Data analysis was performed as we previously described<sup>19</sup>. Genes with an absolute fold-change  $>1.5$  and false discovery rate (FDR)  $< 0.05$  were considered as differentially expressed.

### Statistical analysis

Statistical analyses were conducted using GraphPad Prism 8. A two-tailed Student's *t*-test was used to compare two groups. Ordinal data were analyzed using a two-tailed Mann-Whitney *U* Test. For one independent variable with more than two groups, one-way ANOVA was performed, followed by Tukey's post-hoc test. For scenarios involving two independent variables (factors) with two or more groups, a two-way ANOVA was performed, followed by Tukey's or Sidak's post hoc test to adjust for multiple comparisons, as specified in the figure legends. Grubbs' outlier test was used to determine outliers, which were excluded from final analysis. Data are presented as mean  $\pm$  standard error of the mean (SEM). A *P*-value of 0.05 or less was considered statistically significant. The exact *P* values, as well as the number of independent experiments or biological replicates, are specified in figures and figure legends.

### Reporting summary

Further information on research design is available in the Nature Portfolio Reporting Summary linked to this article.

### Data availability

All data are included in the paper or the Supplementary Information. The raw numbers for charts and graphs, and unedited gel images are available in the Source Data. Additional raw data are available from the authors, as are unique reagents used in this article. The RNA-sequencing data have been deposited in the Gene Expression Omnibus (GEO) repository under the accession code [GSE290443](https://www.ncbi.nlm.nih.gov/geo/query/acc.cgi?acc=GSE290443). Source data are provided with this paper.

### Code availability

Code for RNA-sequencing data analysis is available via the Zhang lab GitHub repository (<https://github.com/hanruizhang/NatCommun-bioRxiv.2024.608411>).

### References

- Doran, A. C., Yurdagul, A., Jr & Tabas, I. Efferocytosis in health and disease. *Nat. Rev. Immunol.* **20**, 254–267 (2019).
- Boada-Romero, E., Martinez, J., Heckmann, B. L. & Green, D. R. The clearance of dead cells by efferocytosis. *Nat. Rev. Mol. Cell Biol.* **21**, 398–414 (2020).
- Sachet, M., Liang, Y. Y. & Oehler, R. The immune response to secondary necrotic cells. *Apoptosis* **22**, 1189–1204 (2017).
- Kawano, M. & Nagata, S. Efferocytosis and autoimmune disease. *Int. Immunol.* **30**, 551–558 (2018).
- Suurmond, J. & Diamond, B. Autoantibodies in systemic autoimmune diseases: specificity and pathogenicity. *J. Clin. Investig.* **125**, 2194–2202 (2015).
- Ma, Y. et al. Efferocytosis in dendritic cells: an overlooked immunoregulatory process. *Front. Immunol.* **15**, 1415573 (2024).
- Mehrotra, P. & Ravichandran, K. S. Drugging the efferocytosis process: concepts and opportunities. *Nat. Rev. Drug Discov.* **21**, 601–620 (2022).
- Herrmann, M. et al. Impaired phagocytosis of apoptotic cell material by monocyte-derived macrophages from patients with systemic lupus erythematosus. *Arthritis Rheum.* **41**, 1241–1250 (1998).
- Baumann, I. et al. Impaired uptake of apoptotic cells into tingible body macrophages in germinal centers of patients with systemic lupus erythematosus. *Arthritis Rheum.* **46**, 191–201 (2002).
- Muñoz, L. E. et al. Remnants of secondarily necrotic cells fuel inflammation in systemic lupus erythematosus. *Arthritis Rheum.* **60**, 1733–1742 (2009).
- Huang, W. N., Tso, T. K., Wu, H. C., Yang, H. F. & Tsay, G. J. Impaired phagocytosis of apoptotic cell material in serologically active clinically quiescent patients with systemic lupus erythematosus. *Int. J. Rheum. Dis.* **19**, 1310–1316 (2016).
- Hu, H. et al. Defective efferocytosis by aged macrophages promotes STING signaling mediated inflammatory liver injury. *Cell Death Discov.* **9**, 236 (2023).
- Boucher, D. M. et al. Age-related impairments in immune cell efferocytosis and autophagy hinder atherosclerosis regression. *Arterioscler. Thromb. Vasc. Biol.* **45**, 481–495 (2025).
- Cohen, P. L. et al. Delayed apoptotic cell clearance and lupus-like autoimmunity in mice lacking the c-met membrane tyrosine kinase. *J. Exp. Med.* **196**, 135–140 (2002).
- Rodriguez-Manzanet, R. et al. T and B cell hyperactivity and autoimmunity associated with niche-specific defects in apoptotic body clearance in TIM-4-deficient mice. *Proc. Natl Acad. Sci. USA* **107**, 8706–8711 (2010).
- Ramirez-Ortiz, Z. G. et al. The scavenger receptor SCARF1 mediates the clearance of apoptotic cells and prevents autoimmunity. *Nat. Immunol.* **14**, 917–926 (2013).
- Asano, K. et al. Masking of phosphatidylserine inhibits apoptotic cell engulfment and induces autoantibody production in mice. *J. Exp. Med.* **200**, 459–467 (2004).
- Hanayama, R. et al. Autoimmune disease and impaired uptake of apoptotic cells in MFG-E8-deficient mice. *Science* **304**, 1147–1150 (2004).
- Shi, J. et al. A genome-wide CRISPR screen identifies WDFY3 as a regulator of macrophage efferocytosis. *Nat. Commun.* **13**, 7929 (2022).
- Dragich, J. M. et al. Autophagy linked FYVE (Alfy/WDFY3) is required for establishing neuronal connectivity in the mammalian brain. *eLife* **5**, e14810 (2016).
- Clausen, B. E., Burkhardt, C., Reith, W., Renkawitz, R. & Förster, I. Conditional gene targeting in macrophages and granulocytes using LysMcre mice. *Transgenic Res.* **8**, 265–277 (1999).
- Mevorach, D., Zhou, J. L., Song, X. & Elkon, K. B. Systemic exposure to irradiated apoptotic cells induces autoantibody production. *J. Exp. Med.* **188**, 387–392 (1998).
- Zheng, Y., Liu, Q., Goronzy, J. J. & Weyand, C. M. Immune aging—a mechanism in autoimmune disease. *Semin. Immunol.* **69**, 101814 (2023).
- Groom, J. R. & Luster, A. D. CXCR3 in T cell function. *Exp. Cell Res.* **317**, 620–631 (2011).
- Westerterp, M. et al. Cholesterol accumulation in dendritic cells links the inflammasome to acquired immunity. *Cell Metab.* **25**, 1294–1304.e1296 (2017).
- Theisen, D. J. et al. WDFY4 is required for cross-presentation in response to viral and tumor antigens. *Science* **362**, 694–699 (2018).
- Guerriero, J. L. Macrophages: their untold story in T cell activation and function. *Int. Rev. Cell Mol. Biol.* **342**, 73–93 (2019).
- Vande Walle, L. & Lamkanfi, M. Drugging the NLRP3 inflammasome: from signalling mechanisms to therapeutic targets. *Nat. Rev. Drug Discov.* **23**, 43–66 (2024).
- Fu, J. & Wu, H. Structural mechanisms of NLRP3 inflammasome assembly and activation. *Annu. Rev. Immunol.* **41**, 301–316 (2023).



30. Hoss, F., Rodriguez-Alcazar, J. F. & Latz, E. Assembly and regulation of ASC specks. *Cell Mol. Life Sci.* **74**, 1211–1229 (2017).
31. Ben-Sasson, S. Z., Wang, K., Cohen, J. & Paul, W. E. IL-1 $\beta$  strikingly enhances antigen-driven CD4 and CD8 T-cell responses. *Cold Spring Harb. Symp. Quant. Biol.* **78**, 117–124 (2013).
32. Peng, Y. & Elkon, K. B. Autoimmunity in MFG-E8-deficient mice is associated with altered trafficking and enhanced cross-presentation of apoptotic cell antigens. *J. Clin. Investig.* **121**, 2221–2241 (2011).
33. Jiang, Q. et al. Role of Th22 cells in the pathogenesis of autoimmune diseases. *Front. Immunol.* **12**, 688066 (2021).
34. Croce, K. R. et al. A rare genetic variant confers resistance to neurodegeneration across multiple neurological disorders by augmenting selective autophagy. *Neuron* (2025).
35. Tang, S. H., Silva, F. J., Tsark, W. M. & Mann, J. R. A. Cre/loxP-deleter transgenic line in mouse strain 129S1/SvImJ. *Genes* **32**, 199–202 (2002).
36. Peña-Martínez, C., Rickman, A. D. & Heckmann, B. L. Beyond autophagy: LC3-associated phagocytosis and endocytosis. *Sci. Adv.* **8**, eabn1702 (2022).
37. Cifone, M. G. et al. Dexamethasone-induced thymocyte apoptosis: apoptotic signal involves the sequential activation of phosphoinositide-specific phospholipase C, acidic sphingomyelinase, and caspases. *Blood* **93**, 2282–2296 (1999).
38. Schilperoord, M. et al. The role of efferocytosis-fueled macrophage metabolism in the resolution of inflammation. *Immunol. Rev.* **319**, 65–80 (2023).
39. Yurdagül, A. Jr et al. ODC (Ornithine Decarboxylase)-Dependent Putrescine Synthesis Maintains MerTK (MER Tyrosine-Protein Kinase) Expression to Drive Resolution. *Arterioscler. Thromb. Vasc. Biol.* **41**, e144–e159 (2021).
40. Ampomah, P. B. et al. Macrophages use apoptotic cell-derived methionine and DNMT3A during efferocytosis to promote tissue resolution. *Nat. Metab.* **4**, 444–457 (2022).
41. Ngai, D., Sukka, S. R. & Tabas, I. Crosstalk between efferocytic myeloid cells and T-cells and its relevance to atherosclerosis. *Front. Immunol.* **15**, 1403150 (2024).
42. Sørensen, K. et al. ALFY localizes to early endosomes and cellular protrusions to facilitate directional cell migration. *J. Cell Sci.* **135**, jcs259138 (2022).
43. Roche, P. A. & Furuta, K. The ins and outs of MHC class II-mediated antigen processing and presentation. *Nat. Rev. Immunol.* **15**, 203–216 (2015).
44. Münz, C. Autophagy beyond intracellular MHC class II antigen presentation. *Trends Immunol.* **37**, 755–763 (2016).
45. Filimonenko, M. et al. Functional multivesicular bodies are required for autophagic clearance of protein aggregates associated with neurodegenerative disease. *J. Cell Biol.* **179**, 485–500 (2007).
46. Filimonenko, M. et al. The selective macroautophagic degradation of aggregated proteins requires the PI3P-binding protein Alf1. *Mol. Cell* **38**, 265–279 (2010).
47. Reinhart, E. F. et al. A highly conserved glutamic acid in ALFY inhibits membrane binding to aid in aggregate clearance. *Traffic (Cph., Den.)* **22**, 23–37 (2021).
48. Yamamoto, A. & Simonsen, A. Alf1-dependent elimination of aggregated proteins by macroautophagy: can there be too much of a good thing?. *Autophagy* **7**, 346–350 (2011).
49. Poon, I. K. H. & Ravichandran, K. S. Targeting efferocytosis in inflammaging. *Annu. Rev. Pharmacol. Toxicol.* **64**, 339–357 (2024).
50. Liebold, I. et al. Apoptotic cell identity induces distinct functional responses to IL-4 in efferocytic macrophages. *Science* **384**, eabo7027 (2024).
51. Better, J. et al. Cell type-specific efferocytosis determines functional plasticity of alveolar macrophages. *Sci. Immunol.* **10**, eadl3852 (2025).
52. Hogquist, K. A. et al. T cell receptor antagonist peptides induce positive selection. *Cell* **76**, 17–27 (1994).
53. Barnden, M. J., Allison, J., Heath, W. R. & Carbone, F. R. Defective TCR expression in transgenic mice constructed using cDNA-based alpha- and beta-chain genes under the control of heterologous regulatory elements. *Immunol. Cell Biol.* **76**, 34–40 (1998).
54. Campisi, L. In vitro antigen-presentation assay for self- and microbial-derived antigens. *Bio Protoc.* **7**, e2307 (2017).
55. Zhang, H. et al. Functional analysis and transcriptomic profiling of iPSC-derived macrophages and their application in modeling Mendelian disease. *Circ. Res.* **117**, 17–28 (2015).
56. Gerlach, B. D. et al. Efferocytosis induces macrophage proliferation to help resolve tissue injury. *Cell Metab.* **33**, 2445–2463.e8 (2021).
57. Moon, H. et al. Crbn modulates calcium influx by regulating Orai1 during efferocytosis. *Nat. Commun.* **11**, 5489 (2020).
58. Wu, X., Wang, Z., Tyler, S. & Zhang, H. Efferocytosis assay to quantify the engulfment and acidification of apoptotic cells by macrophages using flow cytometry. *STAR Protoc.* **5**, 103215 (2024).
59. Ravishanker, B. et al. Tolerance to apoptotic cells is regulated by indoleamine 2,3-dioxygenase. *Proc. Natl Acad. Sci. USA* **109**, 3909–3914 (2012).
60. Shi, H. et al. Loss of TIM4-dependent efferocytosis in Kupffer cells promotes liver fibrosis in nonalcoholic steatohepatitis. *bioRxiv* <https://doi.org/10.1101/2024.01.30.578023> (2024).
61. Trouw, L. A. et al. Anti-C1q autoantibodies deposit in glomeruli but are only pathogenic in combination with glomerular C1q-containing immune complexes. *J. Clin. Investig.* **114**, 679–688 (2004).
62. Moldoveanu, Z. et al. Experimental evidence of pathogenic role of IgG autoantibodies in IgA nephropathy. *J. Autoimmun.* **118**, 102593 (2021).
63. Wang, X. et al. Hepatocyte TAZ/WWTR1 promotes inflammation and fibrosis in nonalcoholic steatohepatitis. *Cell Metab.* **24**, 848–862 (2016).
64. Li, S. et al. STING-induced regulatory B cells compromise NK function in cancer immunity. *Nature* **610**, 373–380 (2022).
65. Golubovskaya, V. & Wu, L. Different subsets of T cells, memory, effector functions, and CAR-T immunotherapy. *Cancers (Basel)* **8**, 36 (2016).
66. Ghosh, M. & Shapiro, L. H. In vitro Ag cross-presentation and in vivo Ag cross-presentation by dendritic cells in the mouse. *Bio Protoc.* **2**, e305 (2012).
67. Kawasaki, T. et al. Alveolar macrophages instruct CD8(+) T cell expansion by antigen cross-presentation in lung. *Cell Rep.* **41**, 111828 (2022).
68. Rawson, P. M. et al. Cross-presentation of caspase-cleaved apoptotic self antigens in HIV infection. *Nat. Med.* **13**, 1431–1439 (2007).
69. Martínez, J. Detection of LC3-associated phagocytosis (LAP). *Curr. Protoc. Cell Biol.* **87**, e104 (2020).
70. Hara, H. et al. Phosphorylation of the adaptor ASC acts as a molecular switch that controls the formation of speck-like aggregates and inflammasome activity. *Nat. Immunol.* **14**, 1247–1255 (2013).
71. Tahtinen, S. et al. IL-1 and IL-1ra are key regulators of the inflammatory response to RNA vaccines. *Nat. Immunol.* **23**, 532–542 (2022).
72. Lang, C. et al. Efferocytosis drives myeloid NLRP3 dependent inflammasome signaling secretion of IL-1 $\beta$  to promote tumor growth. *Front. Immunol.* **13**, 993771 (2022).
73. Yalcinkaya, M. et al. BRCC3-mediated NLRP3 deubiquitylation promotes inflammasome activation and atherosclerosis in Tet2 clonal hematopoiesis. *Circulation* **148**, 1764–1777 (2023).

## Acknowledgements

The authors' research work has received funding from the National Institutes of Health (NIH) (R01HL151611, R01HL168174, P01HL172741, R35HL177389) and the National Center for Advancing Translational

Sciences (NCATS) (Irving Scholar Award through UL1TR001873), the Marjorie and Lewis Katz Scholar Award, and the M. Irène Ferrer Scholar Award (to H.Z.), R35HL145228 (to I.T.), R01NS077111 and R01NS101663 (to A.Y.), the Russell Berrie Foundation Diabetes Scholar Program (to X.W.), the American Heart Association Postdoctoral Fellowship 21POST829654 and Career Development Award 25CDA1451366 (to X.W.), the American Heart Association Postdoctoral Fellowship 20POST35130003 and Career Development Award 23CDA1052177 (to F.L.), and an National Science Foundation (NSF) predoctoral fellowship (to K.R.C.). We would like to acknowledge the NIH funding sources to the Columbia Center for Translational Immunology (CCTI) Flow Cytometry Core by grant number S10OD020056, S10RR027050 and P30DK063608; the NIH/NCI Cancer Center Support Grant P30CA013696 for the use of resources at the Columbia Genome Center; the Columbia Stem Cell Initiative (CSCI) Flow Cytometry Core under the leadership of Michael Kissner; and Nivia M. Urena at the Institute of Comparative Medicine (ICM) for technical support on blood chemistry analyzer. We acknowledge that design elements used in the schematic illustrations in this paper were adapted from publicly available resources provided by the NIAID NIH BIOART collection ([bioart.niaid.nih.gov/bioart](http://bioart.niaid.nih.gov/bioart)).

## Author contributions

X.W. and H.Z. conceived and designed the project. X.W. performed majority of the experiments. Z.W. and J.C. assisted experiments. K.R.C., F.L., and R.K.S. provided technical support. X.W. and H.Z. performed bioinformatic analysis of the RNA-sequencing data. V.D.D. performed pathological and histological assessment. A.Y. established the mouse models for Cre-mediated knockout and overexpression of WDFY3 and provided critical intellectual input to WDFY3 biology. X.W. and H.Z. drafted the paper. I.T. and A.Y. critically read the paper. H.Z. supervised the project and funding. All the authors have read the paper and provided input to the paper.

## Competing interests

Columbia University has filed patent applications related to this work for which K.R.C., A.Y., X.W. and H.Z. are inventors. The remaining authors declare no other competing interests.

## Additional information

**Supplementary information** The online version contains supplementary material available at <https://doi.org/10.1038/s41467-025-63741-3>.

**Correspondence** and requests for materials should be addressed to Xun Wu or Hanrui Zhang.

**Peer review information** *Nature Communications* thanks Jose Crispin, Elvira Mass and the other, anonymous, reviewer(s) for their contribution to the peer review of this work. A peer review file is available.

**Reprints and permissions information** is available at <http://www.nature.com/reprints>

**Publisher's note** Springer Nature remains neutral with regard to jurisdictional claims in published maps and institutional affiliations.

**Open Access** This article is licensed under a Creative Commons Attribution-NonCommercial-NoDerivatives 4.0 International License, which permits any non-commercial use, sharing, distribution and reproduction in any medium or format, as long as you give appropriate credit to the original author(s) and the source, provide a link to the Creative Commons licence, and indicate if you modified the licensed material. You do not have permission under this licence to share adapted material derived from this article or parts of it. The images or other third party material in this article are included in the article's Creative Commons licence, unless indicated otherwise in a credit line to the material. If material is not included in the article's Creative Commons licence and your intended use is not permitted by statutory regulation or exceeds the permitted use, you will need to obtain permission directly from the copyright holder. To view a copy of this licence, visit <http://creativecommons.org/licenses/by-nc-nd/4.0/>.

© The Author(s) 2025